AD-A177 887 A STUDY OF THE GENERATION AND APPLICATION OF RADIATION 1/1
FROM CHANNELED ELECTRONS AND POSITRONS(U) STANFORD UNIV
CA R H PANTELL 28 FEB 86 AFOSR-TR-87-0053
UNCLASSIFIED AFOSR-81-0209 F/G 20/8 NL

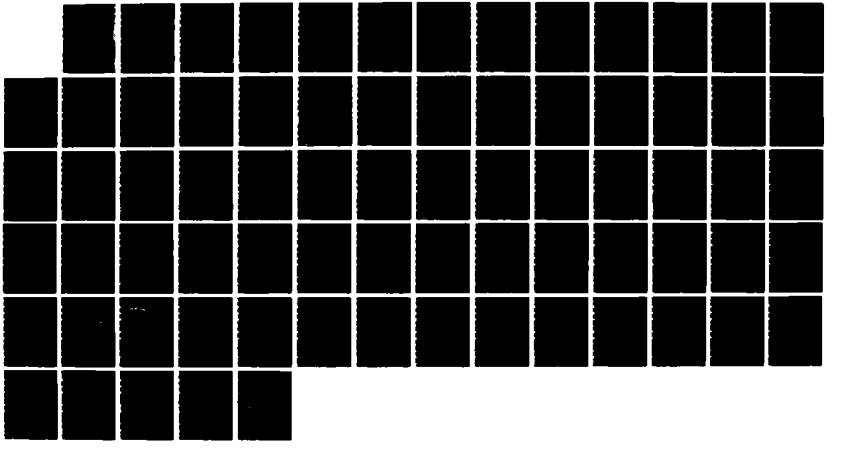

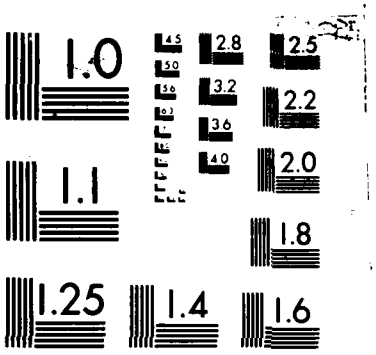

UNCLASSIFIED

SECURITY CLASSIFICATION OF THIS PAGE

REPORT DOCUMENTATION PAGE

1a.	1b. RESTRICTIVE MARKINGS
2a. **AD-A177 007**	3. DISTRIBUTION/AVAILABILITY OF REPORT Approved for public release; distribution unlimited
2b.	
4. PERFORMING ORGANIZATION REPORT NUMBER(S)	5. MONITORING ORGANIZATION REPORT NUMBER(S) AFOSR-TR- 87-0053
6a. NAME OF PERFORMING ORGANIZATION: Stanford University 6b. OFFICE SYMBOL (If applicable):	7a. NAME OF MONITORING ORGANIZATION: AFOSR/NP
6c. ADDRESS (City, State and ZIP Code): Sponsored Projects Office Encina Hall 660 Arguello Way	7b. ADDRESS (City, State and ZIP Code): Bldg 410 Bolling AFB, D.C. 20332-6448
8a. NAME OF FUNDING/SPONSORING ORGANIZATION: AFOSR 8b. OFFICE SYMBOL (If applicable): NP	9. PROCUREMENT INSTRUMENT IDENTIFICATION NUMBER: AFOSR-81-0209
8c. ADDRESS (City, State and ZIP Code): same as 7b.	10. SOURCE OF FUNDING NOS.

PROGRAM ELEMENT NO.	PROJECT NO.	TASK NO.	WORK UNIT NO.
61102F	2301	A8	

11. TITLE (Include Security Classification) "A STUDY OF THE GENERATION AND APPLICATION OF RADIATION FROM CHANNELED ELECTRONS AND POSITRONS", (Unclassified).

12. PERSONAL AUTHOR(S): Dr. Pantell

13a. TYPE OF REPORT	13b. TIME COVERED	14. DATE OF REPORT (Yr., Mo., Day)	15. PAGE COUNT
FINAL	FROM 81/06/01 TO 86/02/28		71

16. SUPPLEMENTARY NOTATION

17 COSATI CODES			18. SUBJECT TERMS (Continue on reverse if necessary and identify by block number)
FIELD	GROUP	SUB. GR.	Channeling, radiation, E-Beams

19. ABSTRACT (Continue on reverse if necessary and identify by block number)

Experiments were conducted to evaluate channeling radiation as a useful source of hard x-rays. The following crystals were studied: LiH, LiD, diamond, BeO, LiF, Si, GaAs, and W. In general, higher-Z materials have intrinsically higher channeling radiation cross sections but they suffer from higher scattering cross sections. It was also found that electron and positron occupation lengths for silicon increase with incident particle energy and are larger for positrons than electrons. Radiation characteristics were also found to be very sensitive to crystal temperature. Encouraging results were obtained when the currents of the incident electron-beams were increased theorectical investigations indicated that strained-layer superlattices could provide a source of x-rays which is comparable in intensity to channeling radiation from ordinary crystals with the additional advantage that it can be tuned by rotating the crystal.

DTIC FILE COPY

20. DISTRIBUTION/AVAILABILITY OF ABSTRACT	21. ABSTRACT SECURITY CLASSIFICATION
UNCLASSIFIED/UNLIMITED X SAME AS RPT ☐ DTIC USERS ☐	UNCLASSIFIED

22a. NAME OF RESPONSIBLE INDIVIDUAL	22b. TELEPHONE NUMBER (Include Area Code)	22c. OFFICE SYMBOL
ROBERT J. BARKER	(202)767-5011	NP

DD FORM 1473, 83 APR EDITION OF 1 JAN 73 IS OBSOLETE.

UNCLASSIFIED

SECURITY CLASSIFICATION OF THIS PAGE

STANFORD UNIVERSITY
STANFORD, CALIFORNIA 94305-6060

SPONSORED PROJECTS OFFICE
ENCINA HALL
660 Arguello Way

Telephone (415) 723-2883
Telex 348 402 Stanfrd STNU

November 20, 1986

Ms. Rene Edwards
AFOSR/PKZA
Department of the Air Force
Building 410
Bolling AFB
Washington, DC 20332

AFOSR-TR- 87-0053

Title: "A Study of the Generation and Application of Radiation From Channeled Electrons and Positrons"
Principal Investigator: Richard H. Pantell
Department: Stanford Electronics Laboratories
SPO Reference Number: 691
Sponsor Reference Number: AFOSR-81-0209

Dear Ms. Edwards:

Enclosed is the Final Scientific Report for the above referenced grant.

To assist with processing, please cite the above SPO Reference Number as well as your reference number when submitting any correspondence regarding this project.

Should you have any questions or require additional information, please call me at (415) 723-2883.

Sincerely,

Steven D. Goode
Contract Officer

SDG/ch
Enclosures

Approved for public release;
distribution unlimited.

AIR FORCE OFFICE OF SCIENTIFIC RESEARCH (AFSC)
NOTICE OF TRANSMITTAL TO DTIC
This technical report has been reviewed and is approved for public release IAW AFR 190-12.
Distribution is unlimited.
MATTHEW J. KERPER
Chief, Technical Information Division

87 2 20 224

A STUDY OF THE GENERATION AND APPLICATION OF RADIATION FROM CHANNELED ELECTRONS AND POSITRONS

Final Scientific Report

1 June 1983 through 28 February 1986

Contract No. AFOSR-81-0209

Prepared for
USAF, Capt. Helen R. Tyson
Department of the Air Force
Bolling Air Force Base, D.C. 20332-6448

Prof. Richard H. Pantell
Principal Investigator
Stanford University
Stanford, CA. 94305

We have performed a number of experiments relevant to the development of channeling radiation (CR) as a useful source of [illegible] X-rays. In one series of experiments, we observed channeling radiation from crystals with atomic numbers ranging from an average of Z=2 (for LiH) to Z=74 (for tungsten.) Higher-Z materials have intrinsically higher channeling radiation cross sections than do lower-Z materials, but they suffer from the disadvantage that the scattering cross section is also higher. Our objective was to learn about the trade-offs involved in using crystals of various atomic numbers. In a second series of experiments, we investigated the effect of thermal vibrations upon channeling radiation spectra. The third objective was to study the production of crystal damage and its effect upon channeling radiation. The fourth and final thrust of our research was an investigation of channeling radiation from alloys and superlattices.

The crystals used in our study of the Z-dependence of channeling radiation included LiH and LiD (Z_{av}=2), diamond, BeO, and LiF (Z_{av}=6), Si (Z_{av}=14), GaAs (Z_{av}=32), and W (Z_{av}=74). We found that, for both electrons and positrons, we could observe channeling radiation from a 300-μm thick LiH crystal, indicating that particles can remain channeled through significant lengths in this material. Channeling radiation emitted by 54-MeV electrons channeled by the (100) planes of LiH and LiD (Z_{av}=2), displayed in Fig. 1, exhibits a number of well-defined spectral peaks. However, the fact that LiH is so low in Z also means that the channeling radiation cross section is quite small. For higher-Z crystals, the tendency is for the occupation length to decrease and for the spectral peaks to broaden. Channeling radiation spectra observed from 17-MeV electrons in the three major planes of GaAs (Z_{av}=32) are displayed in Fig. 2. The occupation length in this case is only 5 μm to 10 μm, and the spectral peaks are relatively broad. In a 90-μm thick tungsten crystal, we were only able to observe a general enhancement of the bremsstrahlung background for electrons, indicating that electrons are dechanneled extremely quickly. On the other hand, we observed intense CR peaks from channeled positrons in tungsten. A fortuitous coincidence of the K-edge of tungsten with the CR peak allowed us to infer an occupation length of the order of 30-μm for 54-MeV positrons.

In order to determine the occupation lengths of electrons and positrons in a crystal with an intermediate value of Z, we measured CR spectra from silicon crystals of a dozen different thicknesses, ranging from 2 μm to 0.8 cm. Data for 54-MeV electrons channeled along the (100) planar direction for four thicknesses are shown in Fig. 3. Several features of these data should be noted. The 2-μm data exhibit line broadening due to the short coherence length, which is limited by the small thickness of the crystal. The 19-μm and 130-μm spectra are typical in that they agree with calculated spectra, and the differences between them are more subtle. The absolute

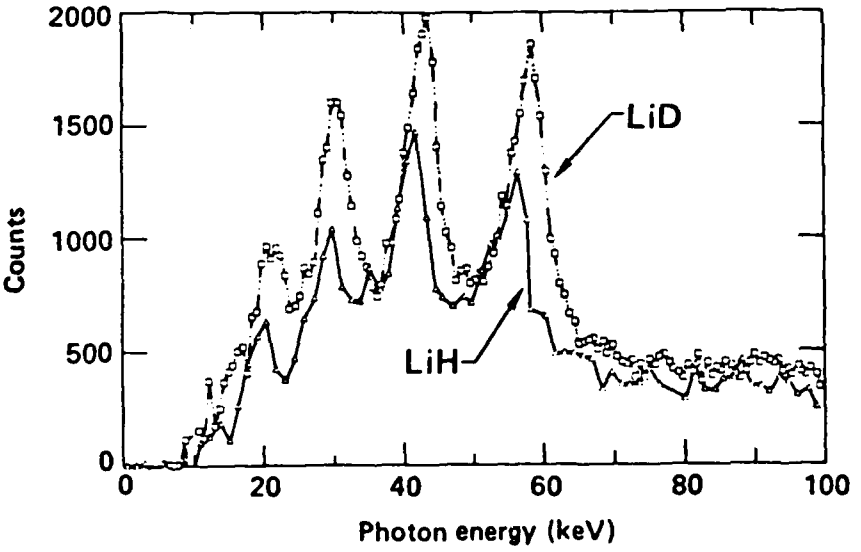

Figure 1: Radiation spectrum emitted by 54 MeV electrons channeled by (100) planes in LiH and LiD.

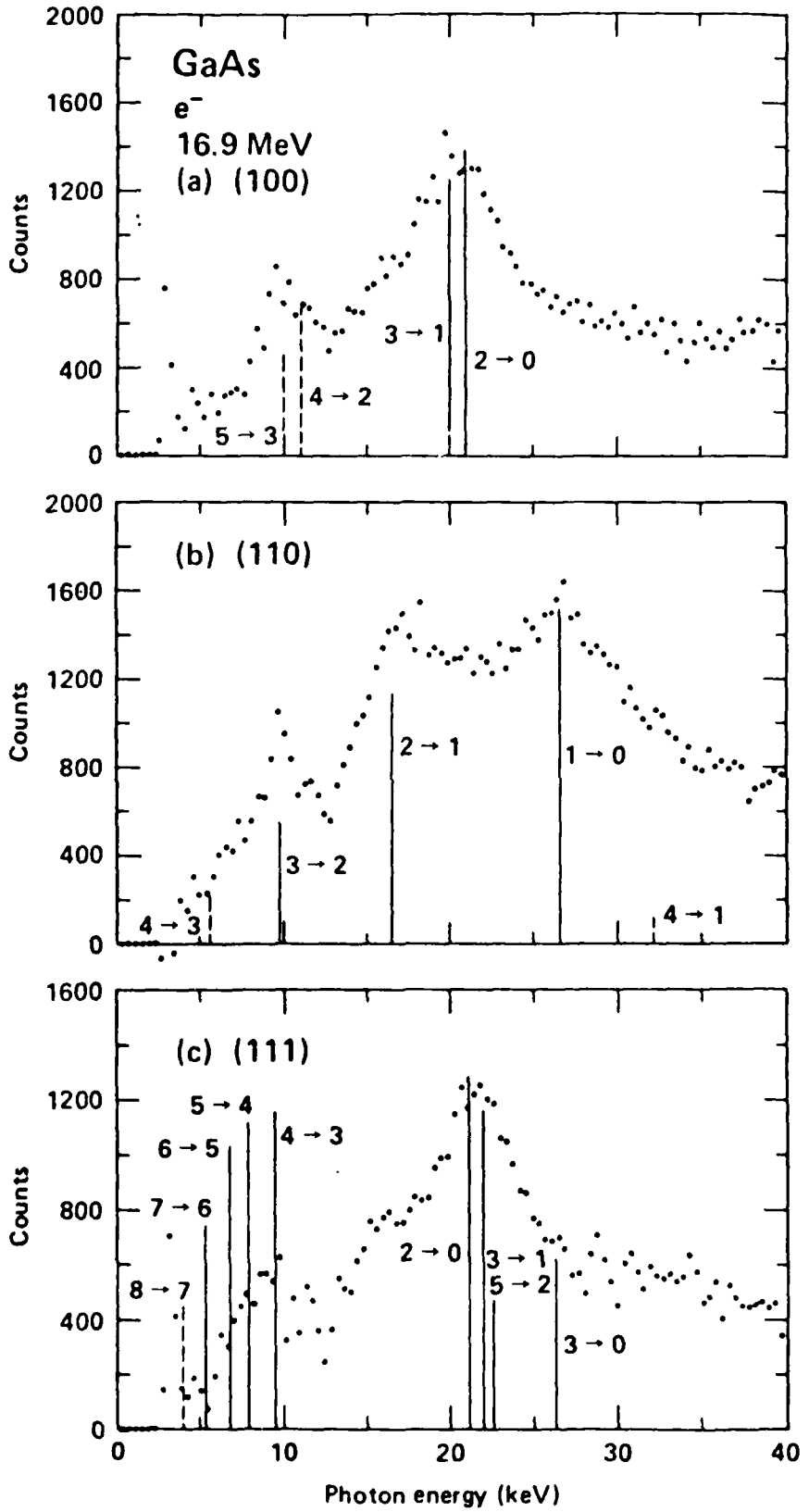

Figure 2: Channeling radiation spectrum from (a) (100), (b) (110), and (c) (111) planes in GaAs using 17 MeV electrons.

Si (100) 54 MeV e^-

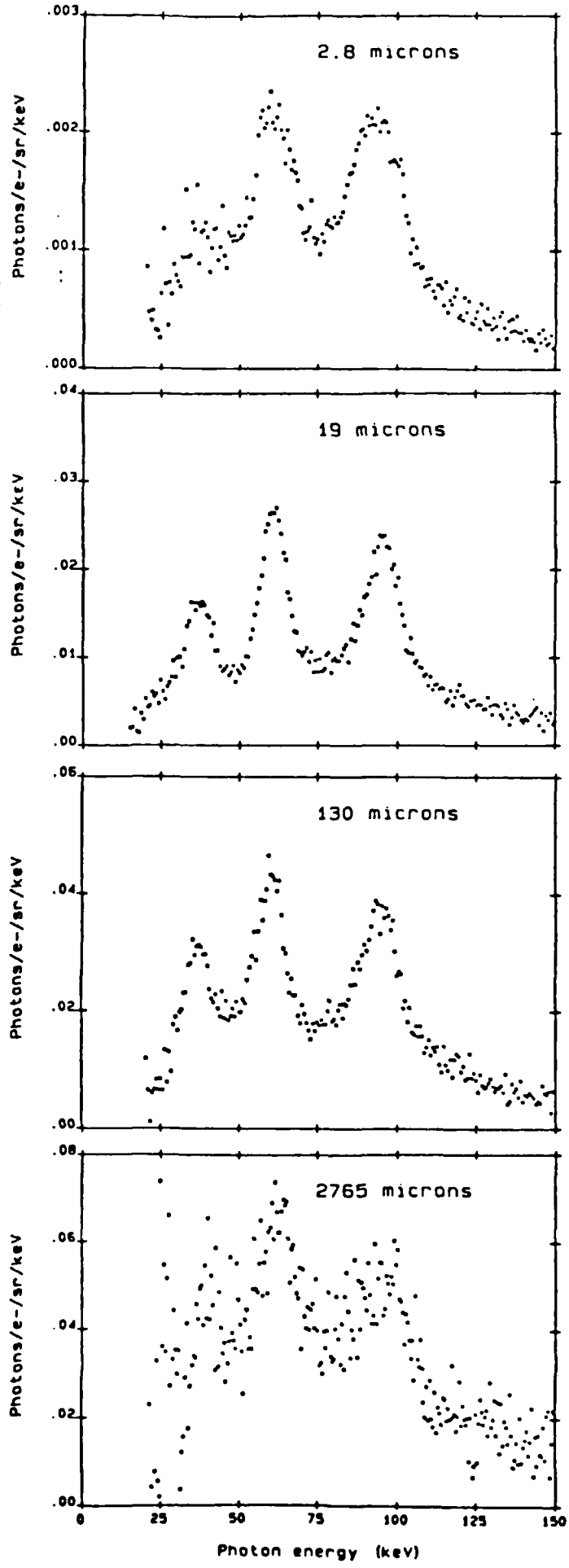

Figure 3:

Emission spectrum from 54 MeV electrons channeled along (100) planes for crystal thicknesses of 2.8, 19, 130 and 2765 microns.

channeling-radiation intensity increases very little between the two, indicating that the bound states have lost a significant fraction of their population after the electrons have penetrated 19 μm. It appears that some more channeling radiation is generated between 130 and 2765 μm, but statistical uncertainties in the background subtraction and calculational uncertainties for the thick-target bremsstrahlung preclude a definitive statement.

These data for silicon crystals having various thicknesses can be used to extract occupation probabilities for channeling eigenstates. Fig. 4 shows the channeling-radiation intensity as a function of crystal thickness for (a) 54-MeV electrons channeled along (100) planes, (b) 54-MeV positrons channeled along (110) planes, and (c) 17-MeV electrons channeled along (110) planes. For these and other cases, we determing the occupation lengths L_{occ} to lie within the range from 16 to 60 μm; our complete results are given in Table 1. We conclude that the occupation lengths for silicon increase with incident charged-particle energy and are larger for positrons than for electrons. In addition to the exponential curves fitted to the data in Fig. 4 that give rise to the 1/e occupation lengths of Table 1, we plot as well the curves corresponding to multiple-scattering fits to the data. Unlike the exponential fits, where the flux is proportional to $1-\exp(-L/L_{occ})$, the multiple-scattering fits vary as $L^{-1/2}$, corresponding to multiple-scattering of the charged particle after the occupied state is partly populated. We see from Fig. 4 that the agreement of the latter with the data is less satisfactory than that of the exponential fits.

Table I: 1/e occupation lengths for silicon

Plane	54-MeV e^-	54-MeV e^+	17-MeV e^-
(100)	24 μm	40 μm	16 μm (n = 1)
(110)	36 μm	60 μm	20, 17, 17 μm (n = 1, 2, 3)
(111)		42 μm	

From our study of the Z-dependence of channeling radiation, we conclude that, for electrons, the best crystal to use as a channeling radiation source would have a fairly low Z -- in the range of 6 to 20. For positrons, however, a higher Z crystal such as tungsten could be used because positrons are much less subject to scattering.

Figure 4: Channeling radiation intensity as a function of crystal - thickness for:

(a)

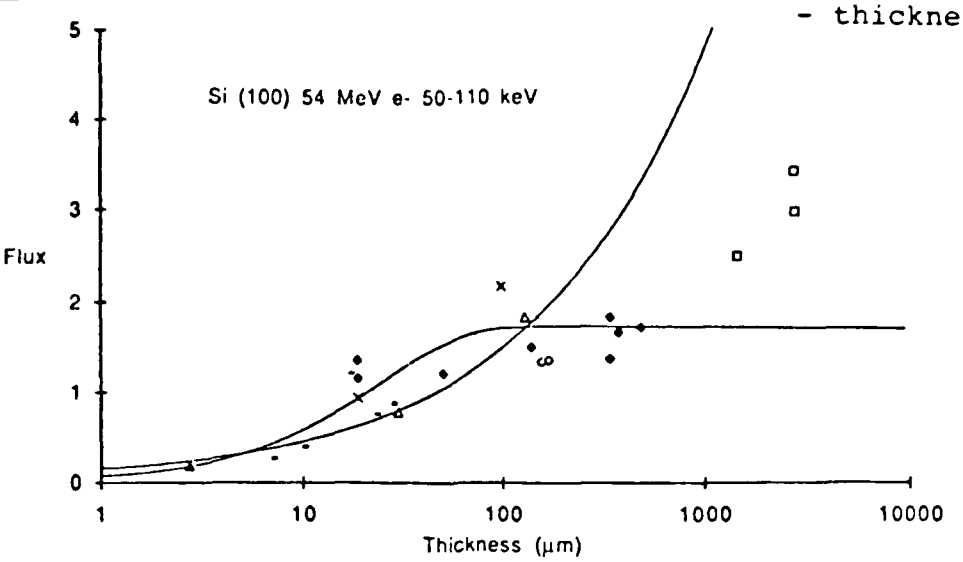

(a) 54 MeV electrons channeled along (100) planes

(b)

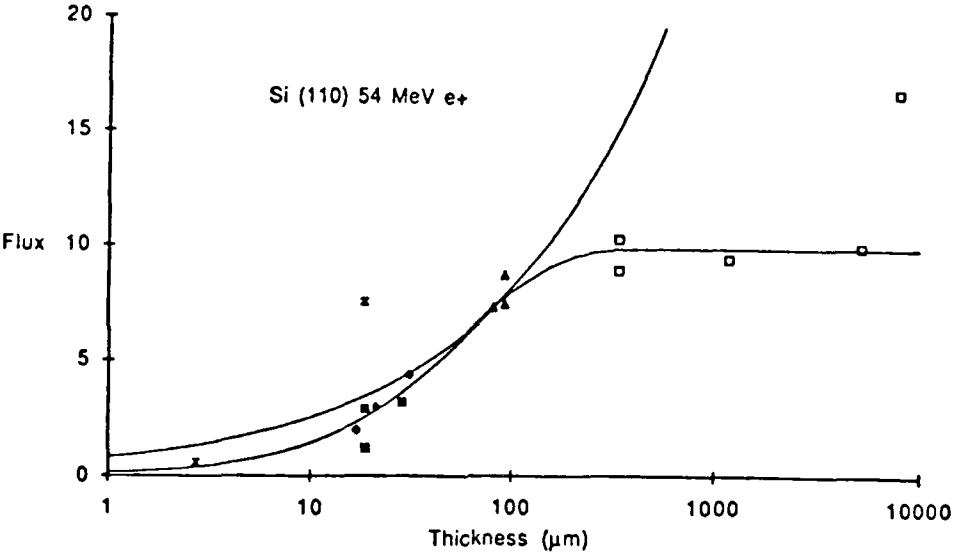

(b) 54 MeV positrons channeled along (110) planes

(c)

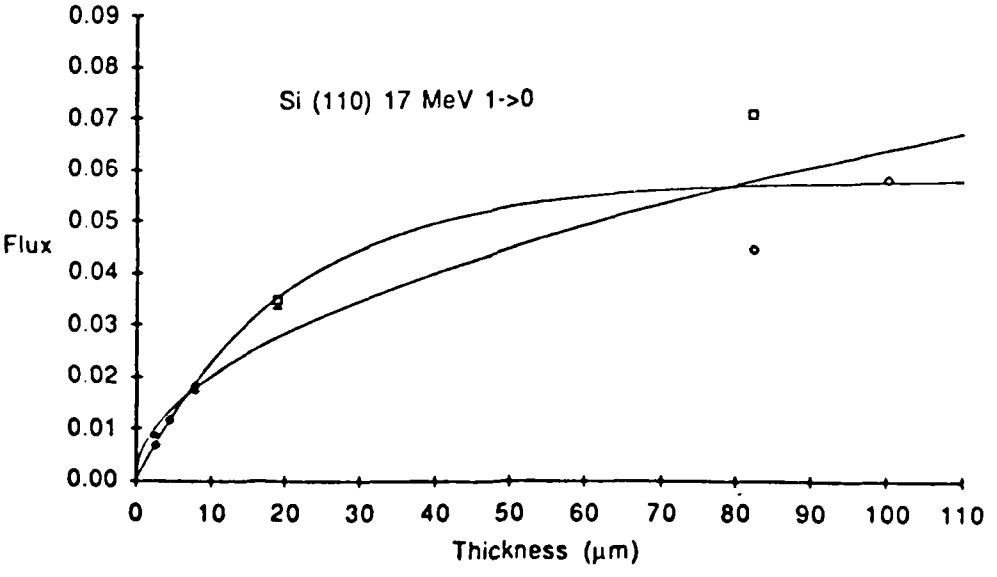

(c) 17 MeV electrons channeled along (110) planes

In order to investigate the effect of thermal vibrations upon channeling radiation, we attached a small refrigerator to a silicon crystal and recorded CR spectra from 54-MeV electrons for a range of temperatures between 77 K and 300 K. As the crystal was cooled, the energies of the $1\rightarrow0$ peaks of both the (110) and (100) planes increased by over 10% and the linewidths decreased substantially (Fig. 5.) When the crystal is cooled, the thermal vibration amplitude decreases, resulting in less thermal smearing of the potential near the atoms and hence a deepening of the potential. The ground state of a channeled electron is most sensitive to the change in the potential, and its energy shifts downward, resulting in a substantial shift in the $1\rightarrow0$ transition energy. (Incidentally, this phenomenon gives us a very sensitive measure of the thermal vibration ampitude and its dependence upon temperature. We inferred a Debye temperature of about 500K for silicon, which is somewhat lower than that obtained from X-ray measurements.)

We studied the effect of thermal vibrations in LiH by a rather novel method. We observed CR emitted by 54-MeV electrons and positrons in both LiH and LiD. 54-MeV electron data from the (100) planes of the two crystals are compared in Fig. 1. The only relevant difference between the two materials should be the thermal vibration amplitude. Since the D atoms are twice as massive as the H atom, their thermal vibration amplitude is less. In effect, LiD should look like cold LiH. Consequently, the energy of the $1\rightarrow0$ transition ought to be greater for LiD than for LiH, while the other peaks ought to be largely unaffected. In fact, we found that the $1\rightarrow0$ peak *does* shift upwards in LiD, but so do the other peaks (albeit to a lesser degree.) This may indicate that, contrary to our expectations, the charge density distribution in LiD is somewhat different from that of LiH.

To date, all of our channeling-radiation measurements have been made at extremely low beam currents (typically in the range of 1pA or even less.) If channeling radiation is to be used as an intense source of hard X-rays, we must use currents beam currents which are at least 6 orders of magnitude more intense than this. This raises two important, related issues: (1) How well can a crystal withstand an intense electron beam? and (2) What is the effect of the induced damage upon the channeling radiation spectrum? In order to gain some insight into these questions, we conducted a third series of experiments in which we intentionally ran intense electron beams through LiF and silicon crystals.

In the first experiment, 54-MeV electrons were injected into three LiF crystals close to the <100> direction at dosages of $5*10^{16}$, $5*10^{17}$, and $5*10^{18}$ electrons/cm^2. Channeling radiation was then observed from 54-MeV planar-channeled electrons and positrons to determine the effects

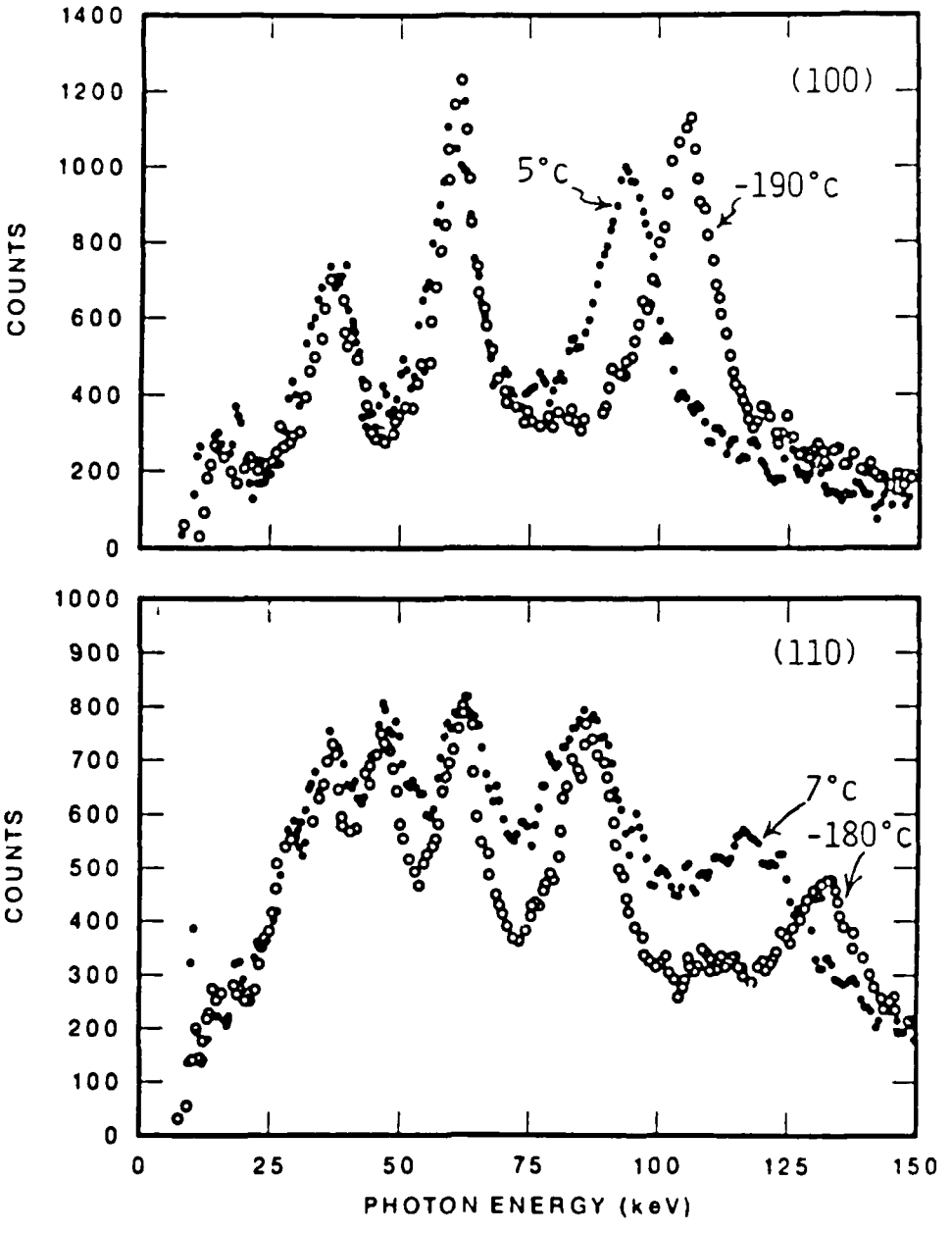

Figure 5 : Radiation from 54.4 MeV electrons at different temperatures of the Si crystal. The upper figure is for (100) planes and the lower one is for (110) planes.

of the induced damage. The channeling radiation spectra from the (110) planes of these three damaged crystals are shown in Fig. 6, along with a (110) spectrum from an undamaged crystal for comparison. The random bremsstrahlung background has been subtracted from each of the three spectra.

As the dosages increase, the spectral peaks become less prominent, eventually disappearing in the crystal with the highest dosage. In addition, the linewidths (determined by fitting Lorentzian-shaped lines) increase with dosage, as shown in Table 2. The cross section σ' for incoherence-induced scattering of a channeled particle is given by

$$\sigma' = \frac{1}{(l_{coh}) * (\text{defect density})}$$

where l_{coh} is the coherence length of a radiating particle. This length may be related to the full-width, half-maximum (FWHM) linewidth $\Delta\omega$ by

$$l_{coh} = \frac{\gamma^2\lambda}{\pi} \frac{\omega}{\Delta\omega}$$

where λ is the wavelength, ω is the frequency, and γ is the ratio of the channeled particle energy to its rest energy. Using the linewidths listed in Table 2 for a dosage of $5*10^{17}$ electrons/cm^2, the value for σ' is $26*10^{-16}$cm^2. This indicates that the cross section presented by an F-center (the most prevalent defect in alkali halides such as LiF) is comparable to the unit cell area.

Table II: Measured linewidths for (110) planar channeling from 54 MeV electrons in damaged LiF crystals.

Transition	$\hbar\omega$ (keV)	FWHM Measured Linewidths for Different Doses (electrons/cm^2)			
		0	$5x10^{16}$	$5x10^{17}$	$5x10^{18}$
$1 \rightarrow 0$	102 keV	15 keV	16 keV	20 keV	–
$2 \rightarrow 1$	75	14	15	17	–
$3 \rightarrow 2$	54	10	12	16	–

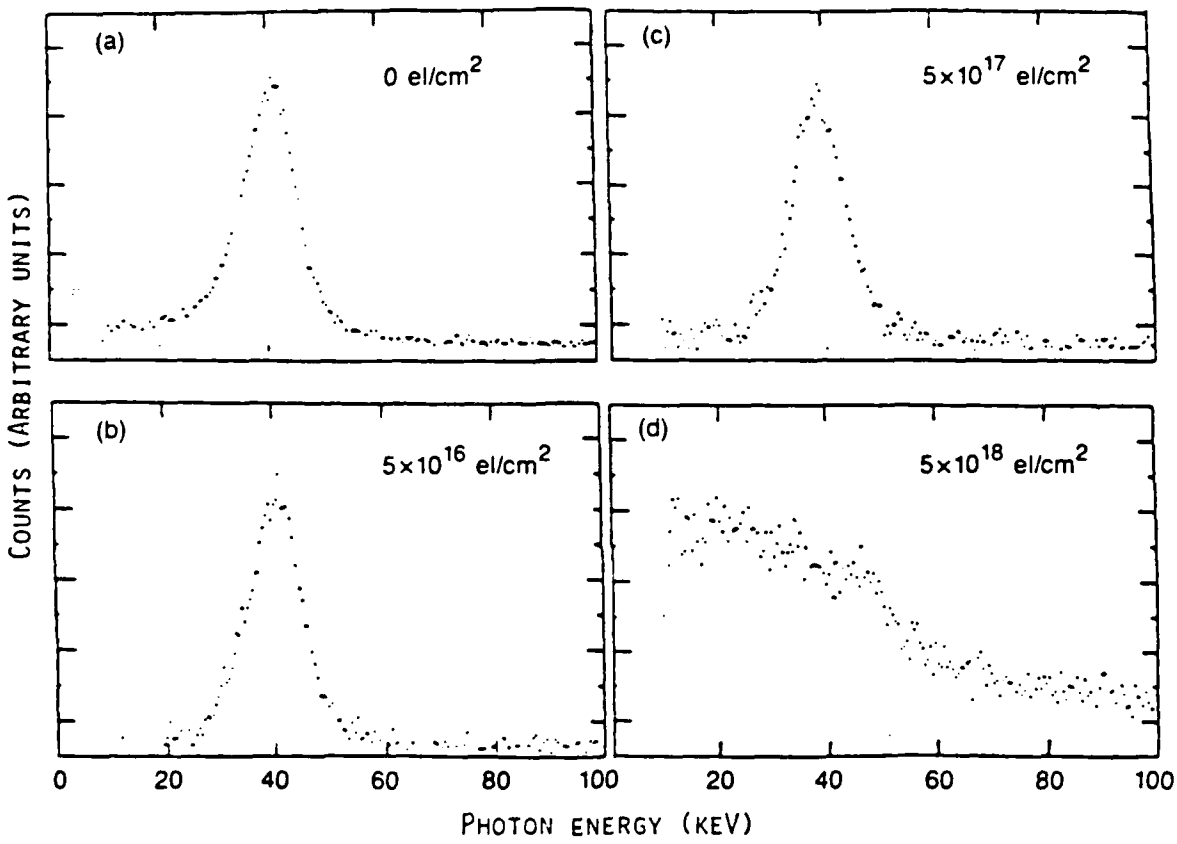

Figure 6: Channeling radiation from 54 MeV positrons channeled by (100) planes in damaged LiF crystals. The electron beam dosages for inducing the damage are indicated in the figure.

Figure 7 shows the channeling radiation obtained from 54-MeV positrons channeled between (100) planes in the same damaged crystals. It is interesting to note that, whereas there is a significant degradation of the electron channeling radiation at a dosage of $5*10^{18}$ electrons/cm^2, there is little change in the shape of the positron emission spectrum. Evidently, the dechanneling cross section is smaller for positrons than for electrons, indicating that the defects may be localized near the atomic planes rather than midway between them.

The high susceptibility of alkali halides to damage by electron beams is well-known. It is clear from the forementioned experiment that one must use crystals which are less susceptible to damage. In a recent experiment, we subjected silicon crystals to somewhat larger doses than those which were used in the LiF experiment. Even for the highest dose, the channeling radiation spectra from electrons suffered no visible degradation -- a very encouraging result.

In our final series of experiments, we have measured channeling radiation spectra from alloys and superlattices. By using an alloy or superlattice rather than a perfect crystal, it is possible to shift channeling radiation peaks by a perceptible amount. Observed and calculated spectra for 16.9 MeV electrons channeled along (111) planes of GaAs, a Ga.7Al.3As alloy, and a Ga.7Al.3As/GaAs superlattice are displayed in Fig. 8. The linewidths are quite large even for intrinsic GaAs because it is a relatively high-Z material; a useful radiation source would necessitate lower-Z alloys. The linewidths for the alloy and the superlattice are larger than that of the intrinsic material; this may reflect the greater disorder in these materials. (In fact, measurements of channeling radiation spectra from alloys and superlattices may provide information about defects, strains, or other imperfections in these materials.)

In addition to these first efforts to study compositional superlattices experimentally, we have developed a theory of channeling radiation from strained-layer superlattices. Our calculations indicate that strained-layer superlattices could provide a source of X-rays which is comparable in intensity to channeling radiation from ordinary crystals with the additional advantage that it can be tuned by rotating the crystal.

Figure 7 shows the channeling radiation obtained from 54-MeV positrons channeled between (100) planes in the same damaged crystals. It is interesting to note that, whereas there is a significant degradation of the electron channeling radiation at a dosage of $5*10^{18}$ electrons/cm^2, there is little change in the shape of the positron emission spectrum. Evidently, the dechanneling cross section is smaller for positrons than for electrons, indicating that the defects may be localized near the atomic planes rather than midway between them.

The high susceptibility of alkali halides to damage by electron beams is well-known. It is clear from the forementioned experiment that one must use crystals which are less susceptible to damage. In a recent experiment, we subjected silicon crystals to somewhat larger doses than those which were used in the LiF experiment. Even for the highest dose, the channeling radiation spectra from electrons suffered no visible degradation -- a very encouraging result.

In our final series of experiments, we have measured channeling radiation spectra from alloys and superlattices. By using an alloy or superlattice rather than a perfect crystal, it is possible to shift channeling radiation peaks by a perceptible amount. Observed and calculated spectra for 16.9 MeV electrons channeled along (111) planes of GaAs, a Ga.7Al.3As alloy, and a Ga.7Al.3As/GaAs superlattice are displayed in Fig. 8. The linewidths are quite large even for intrinsic GaAs because it is a relatively high-Z material; a useful radiation source would necessitate lower-Z alloys. The linewidths for the alloy and the superlattice are larger than that of the intrinsic material; this may reflect the greater disorder in these materials. (In fact, measurements of channeling radiation spectra from alloys and superlattices may provide information about defects, strains, or other imperfections in these materials.)

In addition to these first efforts to study compositional superlattices experimentally, we have developed a theory of channeling radiation from strained-layer superlattices. Our calculations indicate that strained-layer superlattices could provide a source of X-rays which is comparable in intensity to channeling radiation from ordinary crystals with the additional advantage that it can be tuned by rotating the crystal.

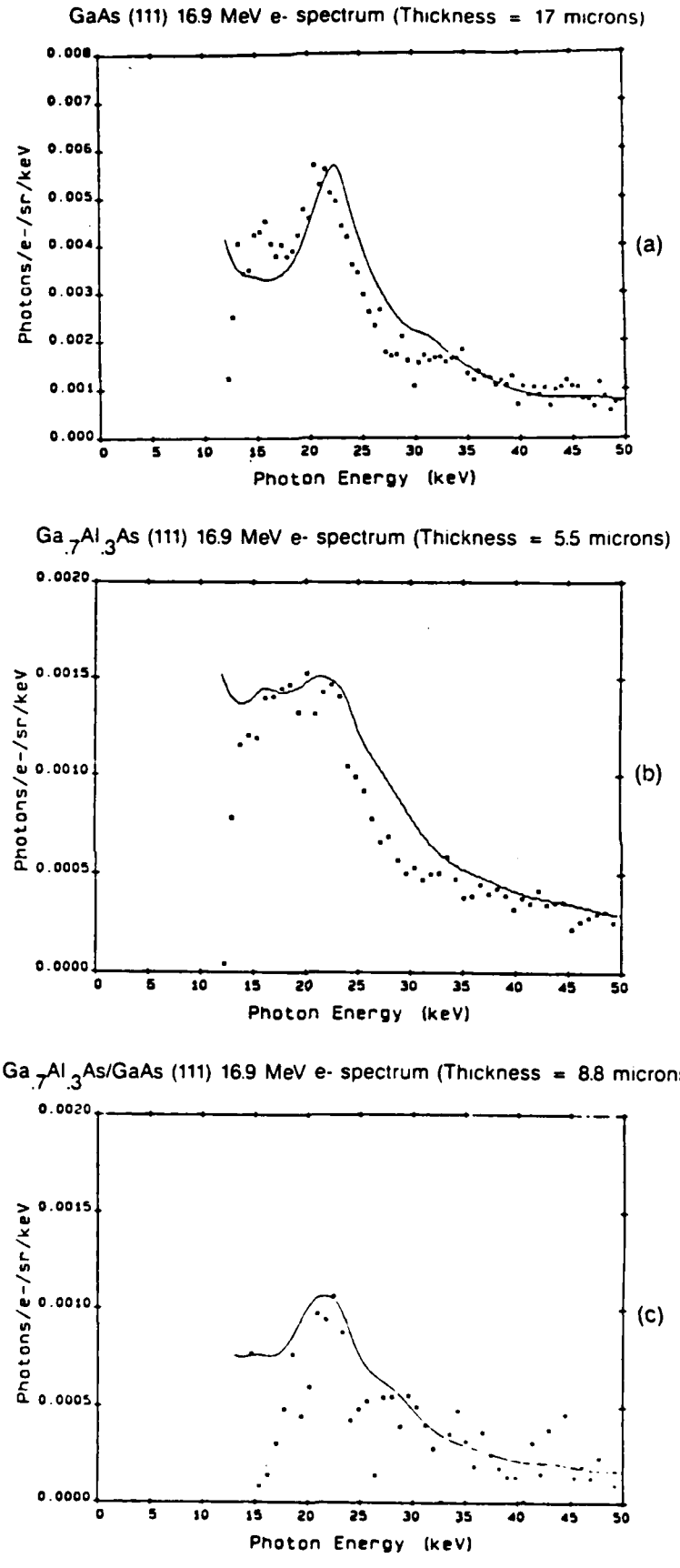

Figure 8: Observed and calculated spectra for 16.9 MeV electron channeling radiation from (111) planes in (a) GaAs, (b) $Ga_{.7}Al_{.3}As$, and (c) $Ga_{.7}Al_{.3}As/GaAs$ superlattice.

THE STUDY OF MATERIAL PROPERTIES USING CHANNELING RADIATION

R.H. Pantell, J.O. Kephart, R.K. Klein
Department of Electrical Engineering
Stanford University
Stanford, CA 94305

H. Park
AT&T Bell Laboratories
1247 South Cedar Crest Blvd.,
Allentown, Pennsylvania 18103

B.L. Berman
Department of Physics
The George Washington University
Washington, DC 20052

S. Datz
Oak Ridge National Laboratory
Oak Ridge, Tennessee 37830

INTRODUCTION

A possible application for channeling radiation is for the investigation of properties of crystals in which the channeling occurs. In this paper we present some general considerations concerning channeling radiation as a measurement technique and describe several specific examples.

I. GENERAL CONSIDERATIONS

Perhaps the first question to pose regarding any measurement procedure is whether or not the procedure alters the properties of the system under observation. In particular, does the channeling cause a significant temperature rise or induce a high density of defects in the crystal?

Under the conditions for which we performed our measurements, the answer to both these questions is "no". We used extremely tenuous electron and positron beams with energies ranging from 10 to 80 MeV. The average current was typically ~ 10^{-13} A over an area of 0.2 cm^2, and the exposure time was of the order of 30 minutes for each channeling radiation spectrum. Under these conditions, the temperature rise in a 20 μm thick Si crystal is less than 2×10^{-4} K, and the fraction of Si atoms displaced by the incident beam is about 1.5 parts in 10^{12}. These effects are negligible.

Table I compares the channeling radiation (CR) technique with three more commonly used methods for studying crystal properties. Channeling radiation complements the other methods, allowing one to make corroborative or perhaps even more accurate measurements of certain properties. The properties measured by channeling radiation are similar to those determined by x-ray diffraction in that parameters are averaged over many lattice sites, whereas electron microscopy and ion channeling are sensitive to point defects and impurities. An interesting feature of channeling radiation as applied to material studies is that electrons and positrons provide different probes. The reason for this is that positrons channel between axes and planes, whereas electrons channel close to axes and planes.

Table I: Some methods for studying crystal properties

Electron Microscopy	Ion Channeling	X-ray Diffraction	Channeling Radiation
High resolution photography Depth limited to ~ 1.0 μm	Location and identification of impurity atoms. Depth limited to ~ 1.0 μm	Measure bulk phenomena: atomic spacing, vibrational amplitudes	Measure bulk phenomena: crystal potentials, vibrational amplitudes.
Uses electrons up to a few MeV in energy.	Uses positive ions in the energy range from a few keV to a few MeV	Information obtained from the intensity of a diffracted wave.	Information obtained from radiation characteristics. Electron or positron energies range from 1.0 MeV to 10 GeV.
Material damage can be a problem.		Can be performed on thick samples.	Sample thicknesses range from μm to mm. Electrons and positrons are different probes.

In Table II, the various radiation parameters are listed, along with crystal properties related to these parameters. As yet, we have used only the first three of these characteristics -- photon energy, spectral linewidth, and intensity -- to obtain information about the crystals. In many cases, the photon energy can be measured to better than one percent accuracy, whereas the linewidth and intensity are determinable to 10-15% accuracy. However, if some crystal characteristic is altered, then a change in linewidth and intensity can be obtained to within several percent.

Table II: Radiation parameters and crystal properties

Radiation Parameter	Crystal Property
Photon energy	Potential function, vibrational amplitude, electronic bonding.
Linewidth	Vibrational amplitude, multiple scattering, defect density.
Intensity	Scattering, potential function.
Time structure	
Direction	
Polarization	

Additional radiation characteristics (time structure, direction, and polarization) may also be used for examining crystals. For example, our linac provides hard x-rays with about 10 psec duration, which could be applied to a study of ultrafast relaxation processes. Streak cameras are sensitive to wavelengths below 1 Å, with a time resolution of 10-20 psec.

At low particle energies, sub-MeV to several MeV, an electron microscope or Van de Graaff accelerator could provide the particles. Below 30 MeV a single klystron linac or a microtron could be used, while a linac would be required for the higher energies. For incident positron or electron energies of a few GeV, the energy of the resulting channeling radiation is a few tens of MeV. Such a source of intense polarized photons in this energy range might be of great importance for photonuclear studies. It is unlikely that a high energy machine would be constructed specifically for channeling radiation studies, but for an existing accelerator the incremental cost is small.

II. MEASUREMENT OF CRYSTAL POTENTIALS

The locations of the emission peaks in the channeling radiation spectra are specified by the crystalline potential function and by the parameters of the incident particle. The crystal potential can be obtained by matching the calculated spectra to some subset of the data.[1] The function so determined can then be checked against the portion of the data that was not used for the matching.

One example concerns the contribution of the covalent bonding electrons in diamond to the potential experienced by a channeled electron.[2,3] We usually calculate the potential of the crystal by adding independent free-atomic or -ionic Hartree-Fock potentials. The "free atom" potential for electrons channeled by (111) planes in diamond is shown in Figure 1, along with another potential derived from x-ray diffraction data. The substantial difference between the two potentials arises from the redistribution of valence electrons (This is four out of six electrons

for each atom in diamond.) associated with the covalent bond, which is not taken into account in the free-atom potential. Eigenvalues are drawn for 30.5 MeV electrons in the x-ray-derived potential well.

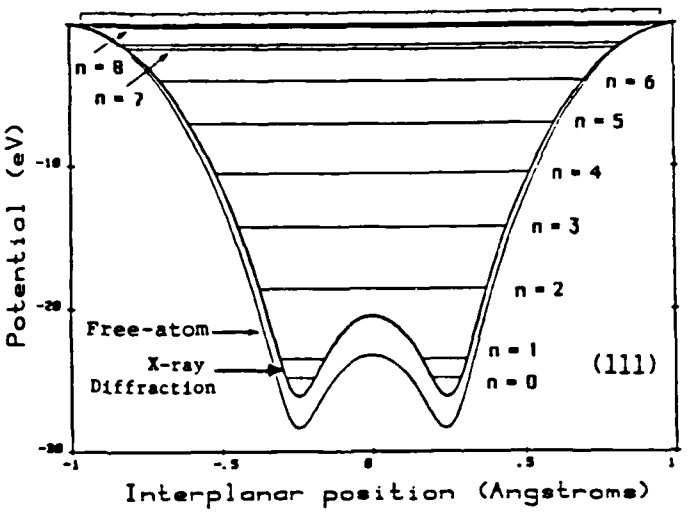

Figure 1: Potential functions for electrons channeled by (111) planes in diamond. X-ray diffraction data include valence electron redistribution, but the free-atom calculation does not.

Figure 2 illustrates the spectra calculated from the two curves in Figure 1 for 30.5 and 54.5 MeV electrons, along with the experimental data. In both instances the x-ray diffraction potential provides a better match to the data. The broad emission peak that occurs at ~ 30 keV in the upper figure and at ~ 60 keV in the lower one is a composite of several $\Delta n = 1$ transitions between the eigenstates of Figure 1. Vibrational motion of the atoms is included in the analysis, both as a Debye-Waller factor and as a line-broadening mechanism. The presence of a $\Delta n = 3$ transition, the $3 \rightarrow 0$ for 30.5 MeV, is apparent in the data.

A new potential was derived by varying parameters so as to obtain the best match between calculated and observed CR transition energies. In Table III a comparison is made between the observed energies and those predicted from the free-atom potential, the x-ray diffraction potential, and a new potential derived by minimizing the sum of the squares of the percent error for each transition. As seen in Figure 3, this new potential is very similar to that derived from x-ray diffraction, with a slightly higher potential midway between the closer set of (111) planes.

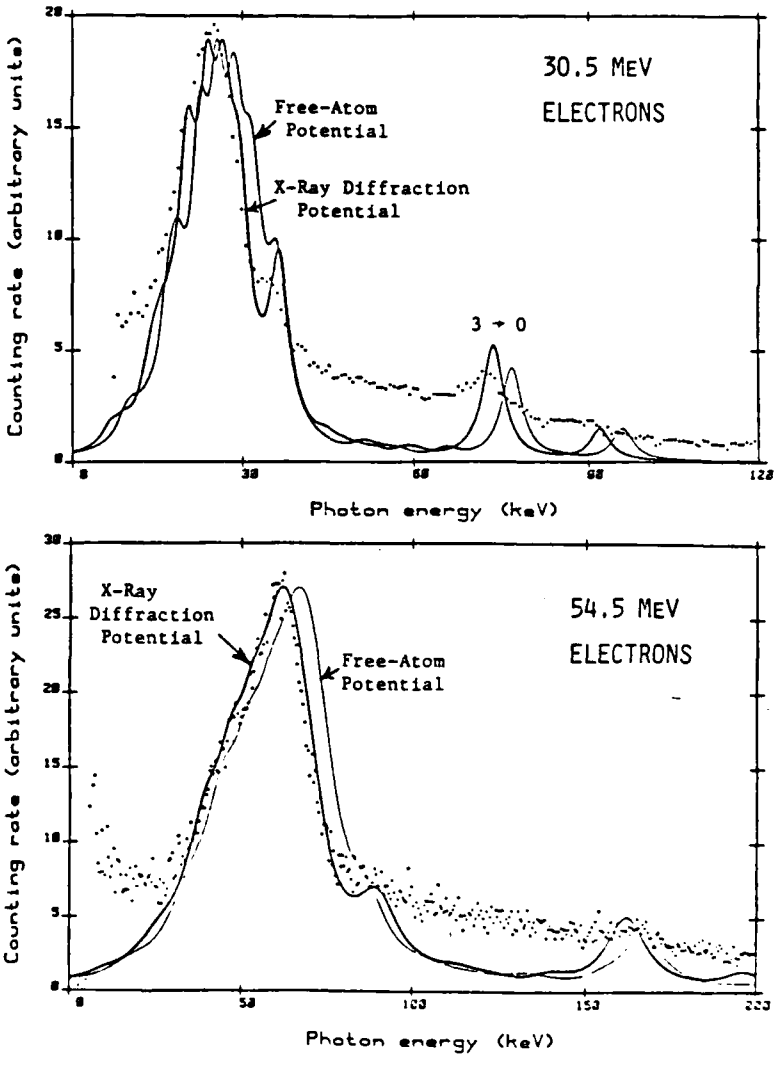

Figure 2: Calculated and measured spectra from (111) planes.

Table III: **Potential calculation based upon minimization of the sum of (percent error)^2 for isolated transitions. The numbers in brackets are the percent errors, and the (% error)^2 has been normalized to unity for the x-ray diffraction potential.**

γ	Transition	Observed Energy (keV)	CALCULATED ENERGY (keV)		
			Using Free-Atom Model	From X-Ray Diffraction Data	From Channeling Radiation Spectra
25.67	2 → 1	9.87	9.85(0.0%)	9.62(-2.6%)	9.75(-1.2%)
25.67	3 → 0	20.6	21.90(6.3%)	20.61(0%)	20.58(-0.1%)
25.67	5 → 0	28.9	31.73(9.8%)	29.48(2.0%)	29.28(1.3%)
34.03	2 → 1	15.1	15.16(0.4%)	14.93(-1.1%)	15.17(0.5%)
34.03	3 → 0	32.5	33.55(3.2%)	31.75(-2.3%)	31.69(-2.5%)
60.76	3 → 0	72.1	76.86(6.6%)	73.59(2.1%)	73.37(1.8%)
Normalized Σ(% Error)^2			7.75	1.0	0.58

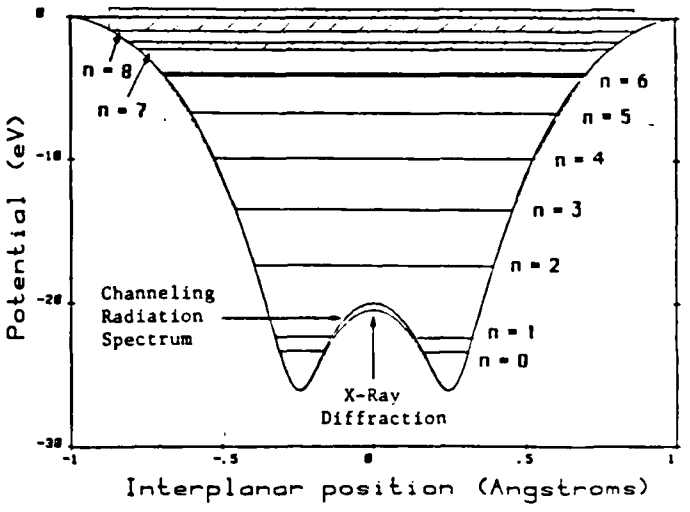

Figure 3: The potential function derived from channeling radiation spectra.

The final check is to compare theory and experiment for a portion of the data not used for error minimization. This is done in Fig. 4 for the data presented in Fig. 2, and it is seen that the spectrum obtained using the new CR-derived potential is essentially indistinguishable from the x-ray-derived calculation, and both are in good agreement with the data. This result indicates that channeling radiation spectra may be used to determine crystalline potential functions to an accuracy comparable to that which can be obtained by using x-ray diffraction.

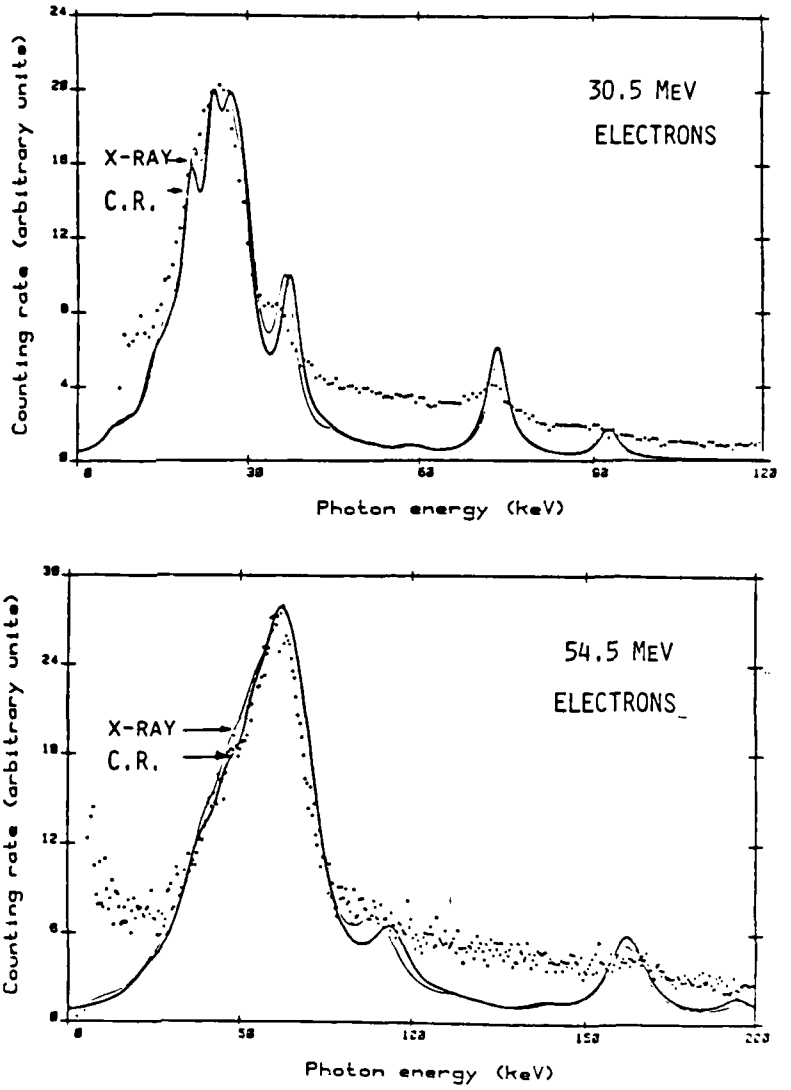

Figure 4: Calculated spectra for X-ray- and CR-derived potentials.

III. OBSERVATION OF PLATELETS IN DIAMOND

In certain types of natural diamond (Type Ia), nitrogen impurities called "platelets" are found in the form of atomic monolayers nucleated on (100) planes. Two proposed models[4,5] for this distortion are illustrated in Fig. 5. A TEM photograph of our Type Ia diamond sample indicated platelet diameters ranging from 40 to 200 Å, with a mean separation of ~ 500Å.

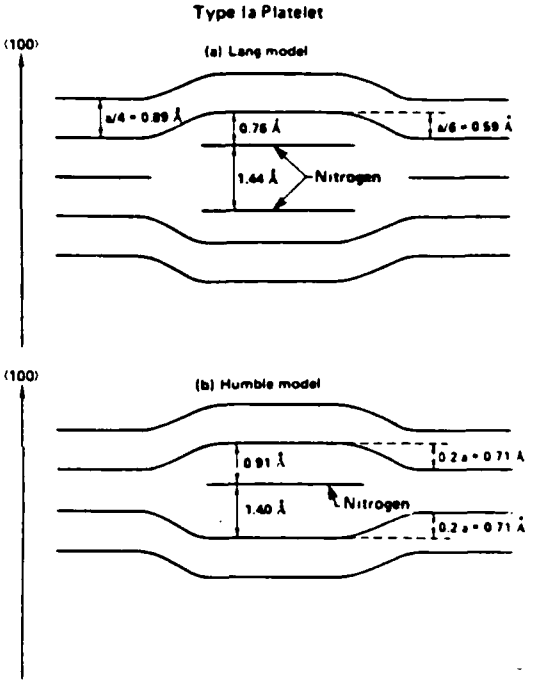

Figure 5: Distortion of (100) planes in diamond due to the presence of nitrogen platelets.

We measured electron channeling radiation from two diamond crystals, one with platelets (Type Ia) and one without platelets (Type IIa.)[6], and the observed photon energies are listed in Table IV. Although there was a significant decrease in the intensity of the emission from the (111) plane, there was essentially no change in the peak photon energy. This is a reasonable result because the platelets cause a stacking-fault type of defect in (111) planes. The only effect of a step discontinuity in an otherwise undistorted plane is to increase the scattering. For the (100) plane, however, the platelets shifted the measured photon energy of the $1 \rightarrow 0$ transition energy downward and broadened the line.

Table IV: Electron channeling radiation from diamond crystals with and without nitrogen platelets.

Plane	Electron Energy	Photon Energy (keV)		
		Type Ia	Type IIa	Calculated
(111)	30.5 MeV	24.2 ± 0.6	25.0 ± 0.5	
(100)	30.5 1 → 0	41.3 ± 0.4	43.0 ± 0.3	43
(100)	54.5 1 → 0	111.0 ± 2	119.8 ± 0.7	122
(100)	54.5 2 → 1	~63	64.7 ± 1.5	63

The platelet-induced downward shift in the 1→0 transition energy is illustrated for the case of 54 MeV electrons in Fig. 6. The maximum emission intensity has been normalized to the same value for both spectra in order to emphasize the difference in photon energies. To account for this frequency shift, it has been assumed that the platelets introduce an uncertainty in the position of the (100) plane, as illustrated in the sketch shown in Fig. 7. The autocorrelation distance along the plane is of the order of the platelet diameter (~100 Å), whereas the periodic length of the wiggling motion is ~2000 Å. This suggests that the usual Debye-Waller factor associated with the thermal vibration amplitude might be augmented by an additional Debye-Waller factor associated with the positional uncertainty of the (100) plane.

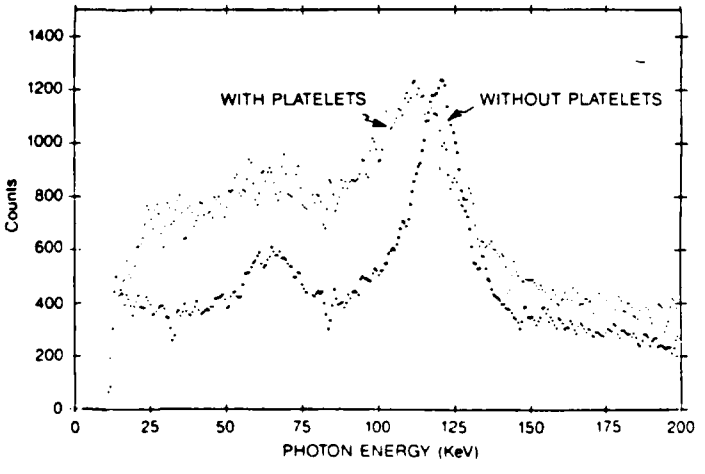

Figure 6: Radiation from 54 MeV electrons channeled along (100) planes.

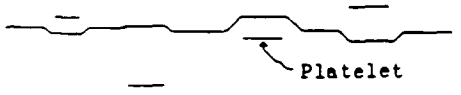

Figure 7: Distortion of (100) planes due to the platelets.

The rms value of the positional uncertainty which yields the best agreement to the data is 0.038 Å. When this is added in quadrature to the thermal vibrational amplitude of 0.042 Å, which was assumed in Table IV, we obtain the potential shown in Fig. 8. Table V contains a tabulation of measured and calculated photon energies using the modified potential function. A positional uncertainty of 0.038 Å is consistent with the measured size and concentration of the platelets, based upon the (100) planar distortion obtained from the models in Figure 5.[6] This result suggests that the effect of the platelets upon the channeled particle may be represented by a Debye-Waller factor, and that the channeling radiation may be used to measure the planar distortion.

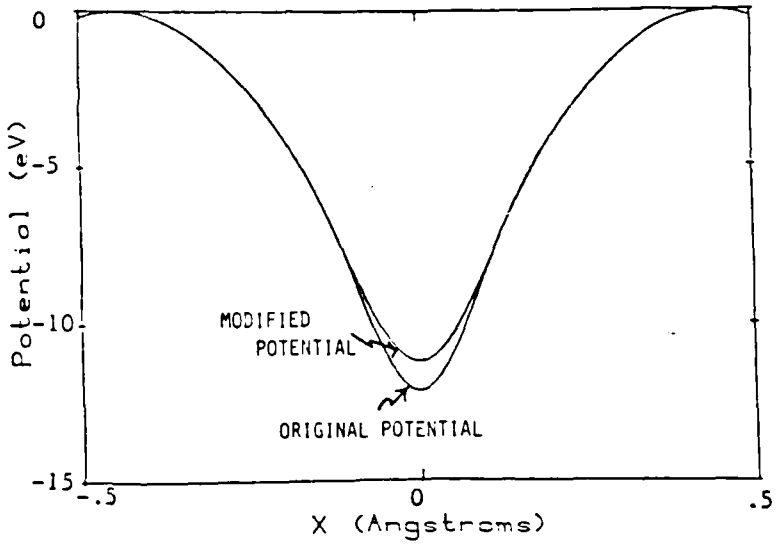

Figure 8: A modified potential function to incorporate the positional uncertainty due to platelets.

Table V: Measured and calculated photon energies from (100) planes in a diamond crystal with platelets. The calculation uses a positional uncertainty of 0.038 Å due to platelets added in quadrature with the 0.042Å vibrational amplitude.

Particle Energy	Measured Emission Energy for Type Ia	Calculated Emission Energy from the Modified Potential
30.5 MeV	41.3 ± 0.4 keV	41 keV
54.5	111 ± 2.0	113
54.5	~ 63	63

IV. DAMAGE EFFECTS IN LiF

It is essential to understand defect production by intense electron and positron beams in various crystals, particularly if one is interested in using CR as a source of x rays.

Fifty-four MeV electrons were injected into three LiF crystals close to the <100> direction at dosages of $5x10^{16}$, $5x10^{17}$, and $5x10^{18}$ electrons per square centimeter. Channeling radiation was then observed from 54 MeV planar-channeled electrons and positrons to determine the effects of the induced damage. The channeling radiation spectra from the (110) planes of these three damaged crystals are shown in Figure 9, along with a (110) spectrum from an undamaged crystal for comparison. The random bremsstrahlung background has been subtracted from each of the four spectra.

As the dosages increase, the spectral peaks become less evident, eventually disappearing in the crystal with the highest dosage. In addition, the linewidths (determined by fitting Lorentzian-shaped lines) increase with dosage, as shown in Table VI.

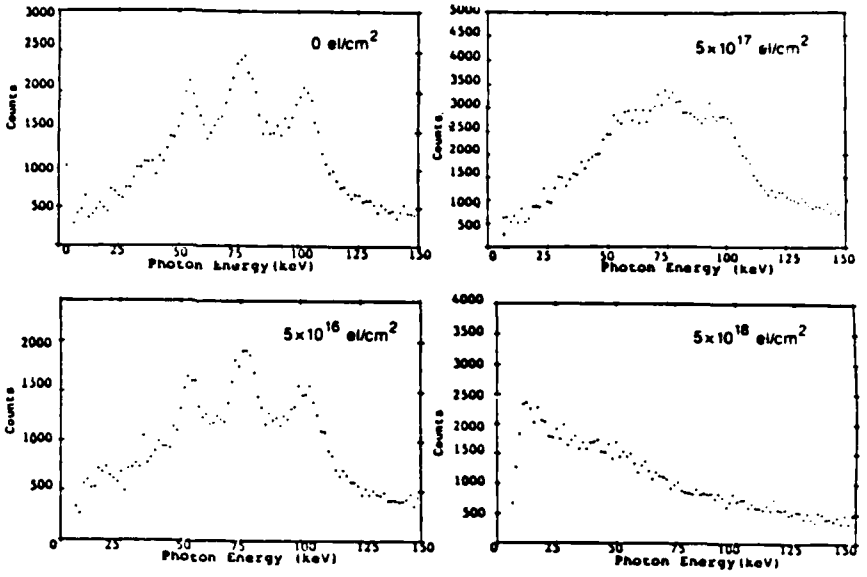

Figure 9: Channeling radiation from 54 MeV electrons channeled by (110) planes in LiF. The crystals were subjected to different dosages of electron beam irradiation: 0 electrons/cm^2, $5x10^{16}$ electrons/cm^2, $5x10^{17}$ electrons/cm^2, and $5x10^{18}$ electrons/cm^2.

Table VI: Measured linewidths for (110) planar channeling from 54 MeV electrons in damaged LiF crystals.

Transition	$\hbar\omega$(keV)	FWHM Measured Linewidths for Different Doses (electrons/cm^2)			
		0	$5x10^{16}$	$5x10^{17}$	$5x10^{18}$
1 → 0	102 keV	15 keV	16 keV	20 keV	-
2 → 1	75	14	15	17	-
3 → 2	54	10	12	16	-

Some of the induced defects are manifested as F-centers, in which the fluorine ion is removed from its site and replaced by an electron. This results in optical absorption, so that an optical absorption spectrum may be used to determine this defect density. Using this procedure, the defect density for the 5×10^{17} electrons/cm^2 dosage was determined to be 1.5×10^{19} cm^{-3}. This gives a cross section σ for F-center formation of

$$\sigma = \frac{\text{defect density}}{(\text{density of F ions})\times(\text{dosage in electrons/cm}^2)}$$

$$= 475\text{b}$$

It is difficult to compare this value with published data,[7] since the available data apply to much lower dosages.

The cross section σ' for incoherence-inducing scattering of a channeled particle by an F-center may be calculated from the formula

$$\sigma' = \frac{1}{(l_{coh})\times(\text{defect density})}$$

where l_{coh} is the coherence length[8] of a radiating particle. This length may be related to the full-width, half-maximum (FWHM) linewidth $\Delta\omega$ by

$$l_{coh} = \frac{\gamma^2\lambda}{\pi}\left(\frac{\omega}{\Delta\omega}\right)$$

where λ is the wavelength, ω is the frequency, and γ is the ratio of the channeled particle energy to its rest energy. Using the linewidths listed in Table VI for a dosage of 5×10^{17} electrons/cm^2, the value for σ' is 26×10^{-16}cm^2.

This value for σ' is extremely large, considering that the lattice constant is 4.0 Å, suggesting that the cross section presented by an F-center is comparable to the unit cell area. One reason for the large value is that the presence of other scattering centers, such as interstitial F ions, has been neglected. Preliminary results we have obtained in damaged silicon indicate that σ' is much smaller for silicon than in LiF.

Figure 10 shows the channeling radiation obtained from 54 MeV positrons channeled between (100) planes in the same damaged crystals. It is interesting to note that, whereas there is a significant degradation of the electron channeling radiation at a dosage of 5×10^{18} electrons/cm^2, there is little change in the shape of the positron emission spectrum. Evidently, the dechanneling cross section σ' is smaller for positrons than for electrons, indicating that the defects may be localized near the atomic planes rather than midway between them.

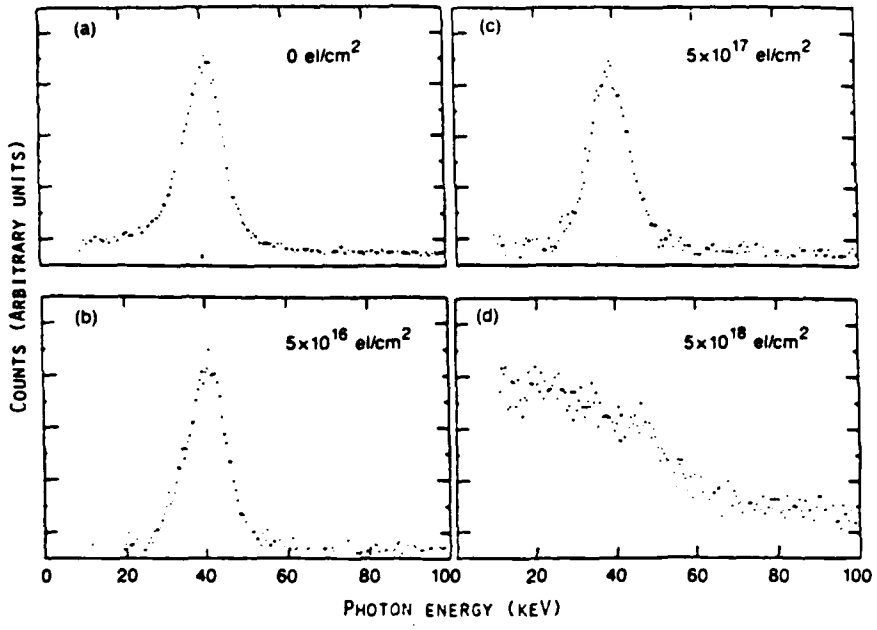

Figure 10: Channeling radiation from 54 MeV positrons channeled by (100) planes in damaged LiF crystals. The electron beam dosages for inducing the damage are indicated in the figure.

V. THERMAL VIBRATION AMPLITUDES

The vibrational motion of the atoms in a crystal affects the crystalline potential, reducing its depth in the vicinity of the atomic planes. This effect is shown in Fig. 11, where (110) planar potentials for electrons in Si are drawn for crystal temperatures of 80 K and 293 K, assuming a Debye temperature of 495 K. (The Debye temperature is a surrogate parameter for vibrational amplitude; a higher value of θ_D corresponding to a smaller amplitude.) Increasing the temperature reduces the well depth and shifts the photon energy of the $1 \rightarrow 0$ transition to lower values. Photon energies for higher transitions are essentially unaffected.

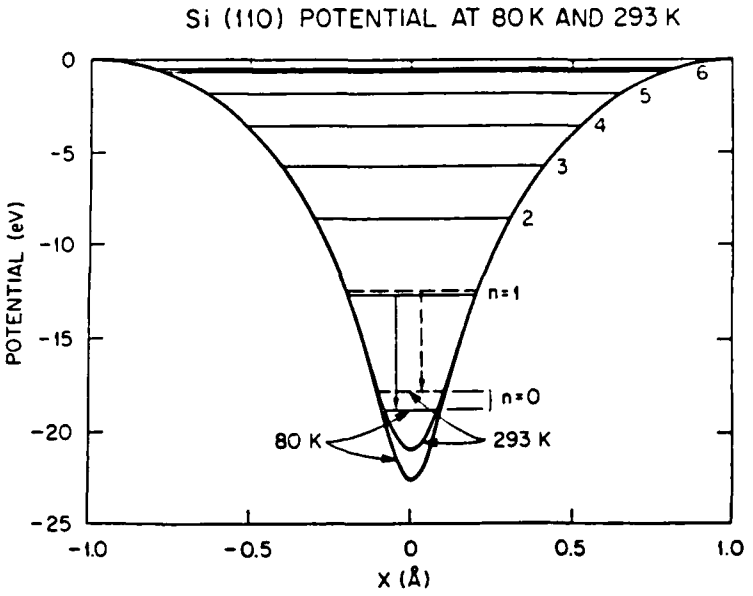

Figure 11: The electron (110) planar potential in Si at temperatures of 80 K and 293 K with an assumed Debye temperature of 495 K. Eigenvalues are shown for 54.4 MeV electrons.

The observed channeling radiation spectra from 54.4 MeV electrons for two planes in Si are presented in Figure 12 for two different temperatures.[9] As anticipated, at higher temperatures the highest peak photon energy (corresponding to the $1 \rightarrow 0$ transition) in the spectrum is reduced, whereas the photon energies for the other transitions are essentially unaffected.

As mentioned previously, the thermal vibration amplitude influences the depth of the potential well (and hence the $1 \rightarrow 0$ photon energy), a relationship which makes it possible to infer the thermal vibration amplitude from the radiation spectrum. Figure 13 shows the measured photon energies for different transitions as a function of crystal temperature, for the (110) planes in Si and 54.4 MeV electrons. The lines drawn through these data points are the calculated energies. For all transitions except the $1 \rightarrow 0$, the predicted values are virtually independent of the Debye temperature θ_D. The agreement between theory and experiment indicates that we have accurately determined the electron energy, and also that the potential function is valid for regions not too close to the atomic planes. Using the measured $1 \rightarrow 0$ transition energies to infer the thermal vibration amplitude as a function of temperature, we obtain a Debye temperature of 495 K, whereas the value obtained from x-ray diffraction data is $\theta_D = 543$ K.

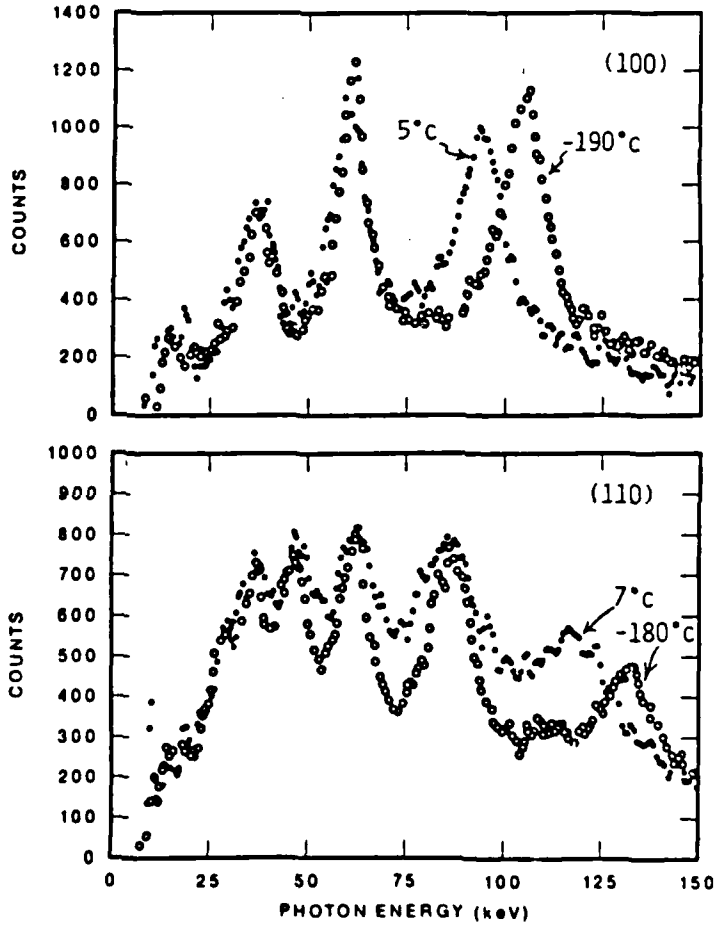

Figure 12: Radiation from 54.4 MeV electrons at different temperatures of the Si crystal. The upper figure is for (100) planes and the lower one is for (110) planes.

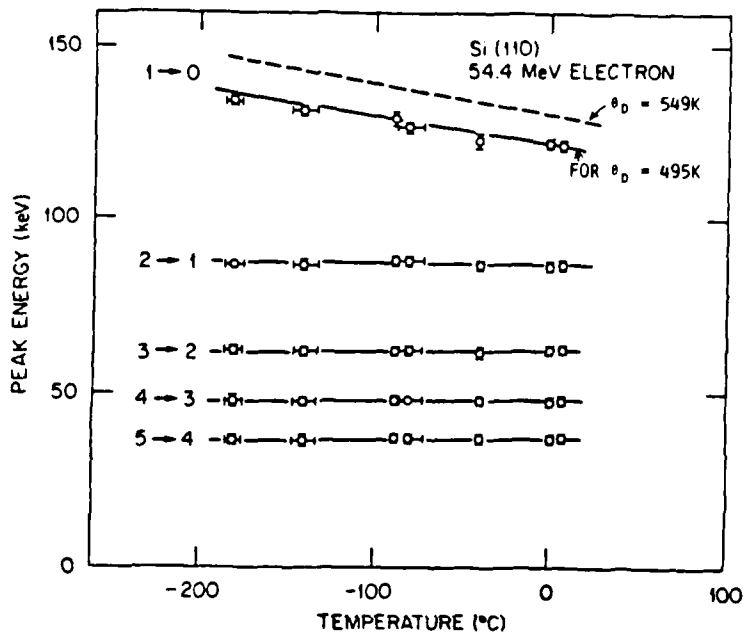

Figure 13: Photons energies emitted by 54.4 MeV electrons channeled by (100) planes in Si as a function of crystal temperature.

It is possible that this discrepancy results from some deficiency in the theoretical treatment of the effect of thermal vibrations upon channeled particles and channeling radiation. If this were true, one would expect similar discrepancies for other crystals with the same structure. Table VII lists measured and calculated $1 \rightarrow 0$ photon energies using the tabulated values for θ_D for four different crystals with the diamond or zincblende structure, including Si. From this table it is seen that there is a much better agreement between theory and experiment for the other three crystals than for Si, despite the fact that the Debye temperatures of the other crystals range both above and below that of Si. The discrepancy that exists for Si is not yet understood.

Table VII: Measured and calculated photon energies from channeling radiation using tabulated values for Debye temperature.

Z	Crystal	Electron Energy (MeV)	θ_D (K)	Vibration Amplitude (Å)	1→0 Transition Energy (keV)			
					110 plane		100 plane	
					Calc.	Meas.	Calc.	Meas.
6	C (Diamond)	54.4	2000	.040	163.7	161 ± 0.5	120.6	119.8 ± 0.7
14	Si	54.4	543	.075	128.5	122.2 ± 1.0	100.0	97.5 ± 1
32	Ge	16.9	290	.085	26.94	27.6 ± 0.5		
31-33	GaAs	16.9	260	.088	26.6	26.6 ± 0.4	20.5	20.6 ± 0.5

VI. CHANNELING RADIATION FROM III-V COMPOUNDS, ALLOYS AND SUPERLATTICES.

We have observed planar channeling radiation emitted by 16.9 MeV electrons from a GaAs crystal, from the alloy $Ga_{.7}Al_{.3}As$, and from the superlattice $Ga_{.7}Al_{.3}As/GaAs$. Each layer of the superlattice is 100 Å thick, and the interfaces are normal to the <100> direction. For the (100) and (110) planes, the direction of relativistic motion was normal to the interfaces.

Figure 14 shows electron planar potentials in GaAs, $Ga_{.7}Al_{.3}As$, and $Ga_{.7}Al_{.3}As/GaAs$, for the (100), (110), and (111) planes. For the superlattice, the potential was calculated by averaging the concentrations of Ga and Al over the layers, so that the potential is equivalent to that of the alloy $Ga_{.85}Al_{.15}As$.

Figure 15 displays the measured and calculated spectra from (111) planes (photons per electron per steradian per keV vs photon energy) for (a) GaAs, (b) $Ga_{.7}Al_{.3}As$, and (c) $Ga_{.7}Al_{.3}As/GaAs$. The sensitivity of the Ge detector decreases substantially below a photon energy of ~ 10 keV, so that data below this energy are not included. Theoretical curves, shown as continuous lines, are based upon an initial 5.5% occupation per state (calculated for an electron beam divergence of 1.5 mrad), and using a different occupation length for each crystal to match the theory with the data. For all three cases the locations of the spectral peaks agree reasonably well with the measured values. In Fig. 15a the occupation length was taken to be 7.0 μm; in Fig. 15b the occupation length was taken to be 2.5 μm; and in Fig. 15c, the superlattice, the occupation length was taken to be 1.5 μm.

We conclude that the occupation lengths of the channeled electrons in the alloy and superlattice are appreciably less than that in the GaAs. A calculation of the eigenstate mismatch at the interfaces of the superlattice indicates that this is not a significant dechanneling mechanism. Perhaps there are residual strains or defects in the alloy and superlattice that contribute to dechanneling, or perhaps the channeling is disrupted by the random introduction of Al atoms.

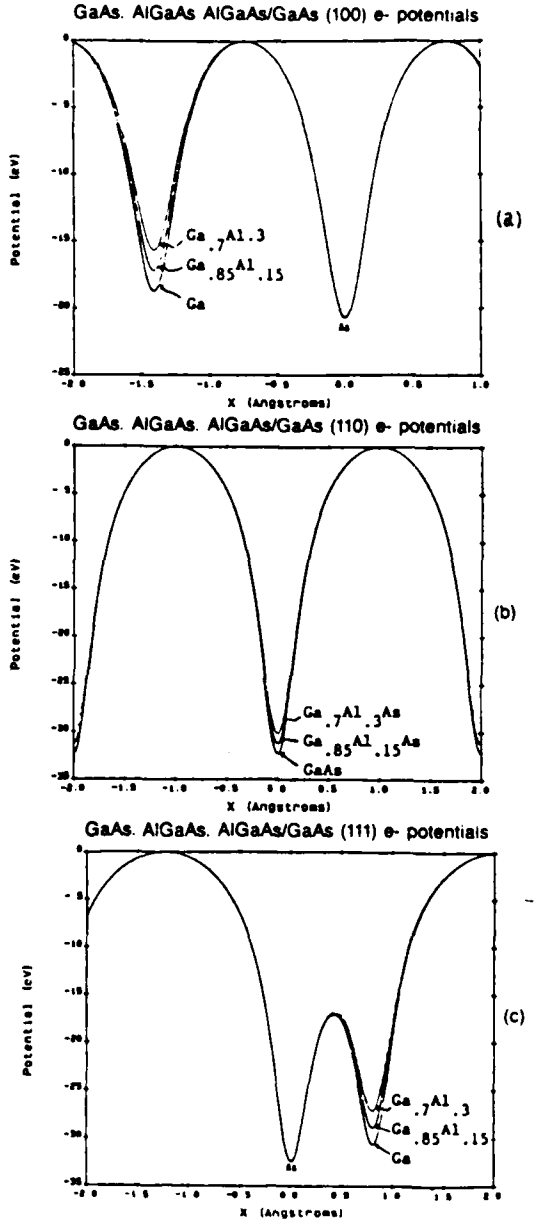

Figure 14: Electron planar potentials for GaAs, $Ga_{.7}Al_{.3}As$, and $Ga_{.7}Al_{.3}As/GaAs$. Figure 14a is for (100) planes, 14b is for (110) planes, and 14c is for (111)planes.

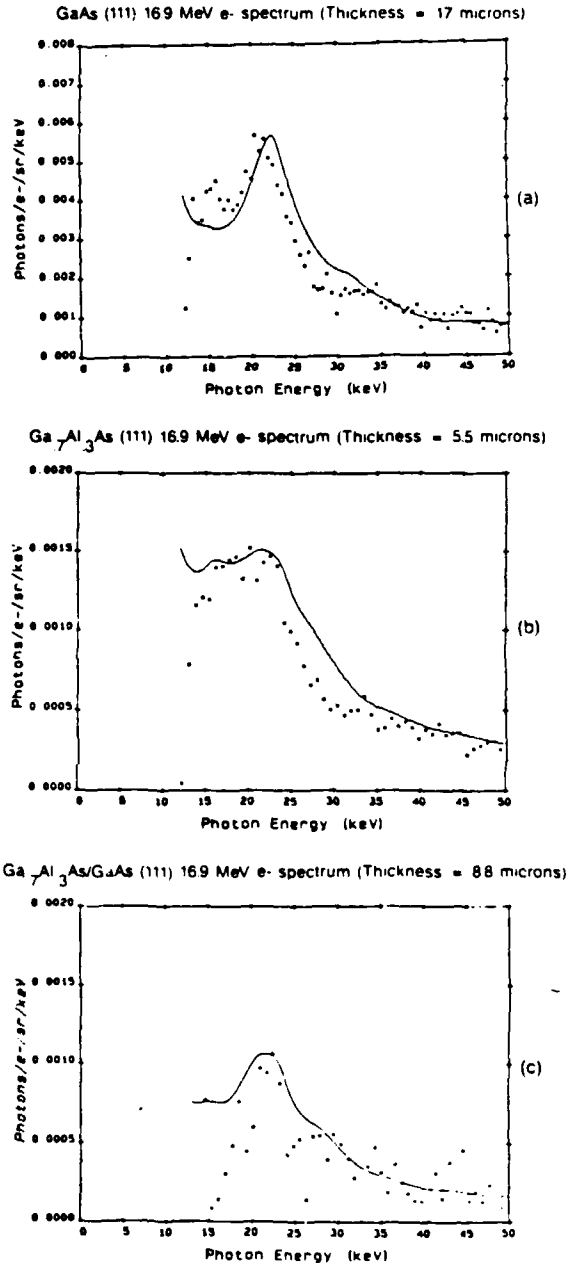

Figure 15: Observed and calculated spectra for 16.9 MeV electron channeling radiation from (111) planes in (a) GaAs, (b) $Ga_{.7}Al_{.3}As$, and (c) $Ga_{.7}Al_{.3}As/GaAs$ superlattice.

VII. OTHER CRYSTAL TYPES AND PROPERTIES

An interesting crystal type to investigate by means of channeling radiation is the strained superlattice,[10] (such as Si: Ge/Si) wherein the lattice constant changes from one layer to the next. A consequence of this is that the normal to a given set of crystal planes may change direction between layers, thereby adding another periodicity to the motion of a channeled particle. This could result in the generation of new frequencies and sidebands in the emission spectrum, which might be used to identify crystal characteristics.

Other suggested study areas include intercalated graphite crystals,[11] in which planes of carbon atoms are separated by a plane of a different atom, and ferroelectrics, where the crystal structure and potential may change with temperature, as in $BaTiO_3$.

This work was supported by the US AFOSR under Contract No. AFOSR81-0209, and by the US Joint Service Electronics Program under Grant No. DAAG29-85K-0048. The electron-positron linac at LLNL received funding from Contract No. W-7405-eng-48, and S. Datz was supported by the US DOE Division of Basic Energy Sciences under Contract No. DE-AC05-840R-21400.

References:

1. R.H. Pantell and R.L. Swent, Appl. Phys. Lett. 25, 910 (1979).
2. J.U. Andersen, S. Datz, E. Laegsgaard, J.P.F. Sellschop, and A.H. Sørenson, Phys. Rev. Lett. 49, 215 (1982).
3. R.K. Klein, Electron Channeling Radiation from Diamond: Theory, Experiments and Applications, Stanford University Ph.D. Thesis, p. 66 (1985).
4. A.R. Lang, Proc. Phys. Soc. London 84, 871 (964).
5. P. Humble, Proc. Roy. Soc. London Ser A. 381, 65 (1982).
6. H. Park, J.O. Kephart, R.K. Klein, R.H. Pantell, B.L. Berman, S. Datz, and R.L. Swent, J. Appl. Phys. 57, 1661 (1985).
7. E. Sonder and L.C. Templeton, Rad. Eff. 16, 115 (1972).
8. J.U. Andersen, K.R. Eriksen, and E. Laegsgaard, Physica Scripta 24, 588 (1981).
9. S. Datz, B.L. Berman, B.A. Dahling, M.V. Hynes, H. Park, J.O. Kephart, R.K. Klein, and R.H. Pantell, Nucl. Instr. and Meth B13, 19 (1986).
10. H. Ikezi, Y.R. Lin-Liu, and T. Ohkawa, Phys. Rev. B 30, 1567 (1984).
11. M.S. Dresselhaus, Physics Today 37, 60 (1984).

Channeling Radiation from GaAs

H. Park, J.O. Kephart, R.K. Klein, and R.H. Pantell
Department of Electrical Engineering
Stanford University
Stanford, CA 94305

B.L. Berman
Lawrence Livermore National Laboratory
University of California
Livermore, CA 94550
and
Department of Physics
The George Washington University
Washington, DC 20052

S. Datz
Oak Ridge National Laboratory
Oak Ridge, TN 37830

Abstract

Channeling-radiation spectra have been obtained from a GaAs crystal with 16.9-MeV electrons and with 54.4-MeV electrons and positrons. Theoretical calculations are in reasonably good agreement with the experimental results.

Because of its application to high-speed electronic devices, gallium arsenide (GaAs) has recently come under extensive study.[1,2] In this letter we report experimental measurements of channeling-radiation spectra from GaAs as a means of obtaining information on the interplanar crystalline potentials. Gallium arsenide has a cubic sphalerite (zincblende) lattice. This structure possesses fcc translational symmetry, with one GaAs molecule per unit cell. One atom is located at (0,0,0) and the other at ($1/4$, $1/4$, $1/4$) of the cube, with a lattice constant equal to 5.65325 ± 0.00002 Å (Ref. 1).

The experiments were carried out with 16.9-MeV (γ = 34.0) electrons and 54.4-MeV (γ = 107.5) electrons and positrons from the Lawrence Livermore National Laboratory Electron-Positron Linear Accelerator incident upon a 25-μm thick GaAs crystal. Details of the experimental apparatus and procedures are given in Ref. 3.

The interplanar potentials for the major crystalline planes in GaAs were calculated from the Doyle-Turner coefficients (Ref. 4), modified by the Debye-Waller factor to account for the thermal vibrations of the atoms. We used a one-dimensional mean-square vibration amplitude $\langle u^2 \rangle$ = 0.0076 Å^2 for both Ga and As (Ref. 5). From the potential function, energy levels were calculated with the many-beam formalism (Ref. 6).

Figure 1 shows the calculated planar potentials and eigenvalues for 16.9-MeV electrons in GaAs. For the (100) and (111) planes the Ga and As atoms are in segregated planes; thus the atomic number Z for the planes alternates between 31 (for Ga) and 33 (for As). The (110) planes contain equal numbers of Ga and As atoms, giving an average atomic charge of 32, so that the potential is quite similar to that for a germanium (Ge) crystal (Ref. 7).

Figure 2 shows the experimental results for the three cases of Fig. 1, together with the calculated energies and strengths of the spectral peaks. Each of the experimental spectra was obtained by subtracting a spectrum taken in a random direction from a spectrum taken in the planar-channeling direction. The positions of the vertical lines in Fig. 2 mark the locations of the calculated transition energies, and the heights of these lines are proportional to the calculated dipole transition intensities. The dashed lines indicate transitions that are initiated from a level near the top of a potential well, and thus are likely to be less intense than shown. The calculated energies of the spectral lines are in good agreement with the experimental data for all three planes. Owing to the rapid decrease of efficiency of the photon detector below 10 keV, the calculated intensities do not match well with the measured ones in this low energy range.

Figure 3 shows the same potentials as in Fig. 1, but this time with the eigenvalues for 54.4-MeV (γ = 107.5) planar-channeled electrons. The number of bound states increases as $\sqrt{\gamma}$ (Ref. 8), as can be seen from a comparison of Figs. 1 and 3. Figure 4 shows the measured spectra for the latter case. Because of the high density of states, coupled with increased line broadening at the higher electron energy, it is not possible to resolve distinct transitions in these spectra. We do note, however, that the calculated strength of the low-energy cluster of transitions for the (111) case [Fig. 4 (c)] is now in agreement with the data.

We also obtained 54.4-MeV positron channeling-radiation spectra for the (100) and (110) planes, for which the calculated potentials and eigenvalues are shown in Fig. 5. Figure 6 shows the measured spectra for these cases. The observed peak energies are about 15% lower than the centroids of our calculated values; this is an effect that has been seen for other crystals as well,

namely, diamond (Ref. 9), Si, Ge (Ref. 7), LiF (Ref. 10), and W (Ref. 11). The reason for this behavior is not yet understood, and further investigation is needed.

Both the electron and positron channeling-radiation spectra from GaAs (110) planes are almost identical to the corresponding Ge spectra (Ref. 7). This is reasonable, since the period of the channeling motion is large compared to the atomic spacing, and thus, to a good approximation, the potential seen by the charged particles is averaged over many atomic sites.

This work was performed at Lawrence Livermore National Laboratory under the auspecies of the U.S. Department of Energy under contract No. W-7405-ENG-48 and was supported as well by the U.S. Air Force Office of Scientific Research under Grant No. AFOSR 81-0209, by the U.S. Joint Services Electronics Program under Grant No. DAAG-29-84-K-0047, and by the U.S. Department of Energy, Division of Basic Energy Sciences, under Contract No. DE-AC05-840R21400 with Martin Marietta Energy Systems, Inc..

References:

1. J.S. Blakemore, J. Appl. Phys. 53, R123 (1982).
2. R.C. Eden, A.R. Livingston, and B.M. Welch, IEEE Spectrum, p. 30 (Dec., 1983); H. Morkoc and P.M. Solomon, IEEE Spectrum, p. 28 (Feb., 1984).
3. R.K. Klein, J.O. Kephart, R.H. Pantell, H. Park, B.L. Berman, R.L. Swent, S. Datz, and R.W. Fearick, Phys. Rev. B: 31, 68 (1985).
4. P.A. Doyle and P.S. Turner, Acta. Cryst. A24, 390 (1968).
5. International Tables for X-ray Crystallography, edited by N.F.M. Henry and K. Lonsdale (Kynoch Press, Birmingham, 1959) Vol. III, p. 241.
6. J.U. Andersen, K.R. Eriksen, and E. Laegsgaard, Phys. Scripta 24, 588 (1981).
7. H. Park, R.L. Swent, J.O. Kephart, R.H. Pantell, B.L. Berman, S. Datz, and R.W. Fearick, Phys. Lett. 96A, 45 (1983).
8. R.H. Pantell and M.J. Alguard, J. Appl. Phys. 50, 798 (1979).
9. S. Datz, R.W. Fearick, H. Park, R.H. Pantell, R.L. Swent, J.O. Kephart, R.K. Klein, and B.L. Berman, Phys. Lett. 96A, 314 (1983).
10. B.L. Berman, S. Datz, R.W. Fearick, J.O. Kephart, R.H. Pantell, H. Park, and R.L. Swent, Phys. Rev. Lett. 49, 474 (1982).
11. W. Beezhold, T.W.L. Sanford, H. Park, J.O. Kephart, R.K. Klein, R.H. Pantell, B.L. Berman, and S. Datz, submitted to J. Appl. Phys.

Table I: GaAs channeling-radiation transition energies for 16.9-MeV electrons.

Plane	Transition	Calculated energy	Measured energy
(100)	2 → 0	21.0	20.6 ± 0.5
	3 → 1	20.0	
	4 → 2	11.1	10.1 ± 0.4
	5 → 3	10.0	
(110)	1 → 0	26.6	26.6 ± 0.4
	2 → 1	16.5	16.7 ± 0.4
	3 → 2	9.8	9.9 ± 0.2
	4 → 3	5.7	No observable peak
(111)	3 → 0	26.3	Broad bump centered at 21.7 keV
	5 → 2	22.6	
	3 → 1	22.0	
	2 → 0	21.2	
	4 → 3	9.5	Broad bump centered at 8.9 keV
	5 → 4	7.9	
	6 → 5	6.8	
	7 → 6	5.4	
	8 → 7	3.7	

Table II: GaAs channeling-radiation transition energies for 54.4-MeV electrons.

Plane	Transition	Calculated energy	Measured energy
(100)	2 → 0	143.9	Broad bump centered at ~90 keV
	3 → 1	139.0	
	4 → 2	107.2	
	5 → 3	102.2	
	6 → 4	75.6	
	7 → 5	69.9	
	8 → 6	51.0	
	9 → 7	41.4	
	9 → 8	24.0	
(110)	6 → 3	185.1	Broad bump centered at ~95 keV
	1 → 0	175.7	
	2 → 1	138.7	
	7 → 4	138.7	
	3 → 2	105.3	
	4 → 3	79.8	
	5 → 4	60.2	
	6 → 5	45.1	
	7 → 6	33.4	
(111)	2 → 0	155.9	Broad bump centered at ~90 keV
	8 → 5	154.9	
	6 → 3	154.1	
	3 → 1	148.0	
	5 → 2	141.0	
	7 → 4	136.0	
	4 → 2	110.2	
	5 → 3	102.8	
	6 → 4	82.0	
(111)	7 → 6	54.1	Broad bump centered at ~35 keV
	6 → 5	51.2	
	8 → 7	50.0	
	9 → 8	43.6	
	10 → 9	41.1	
	11 → 10	38.5	
	12 → 11	34.3	
	13 → 12	28.7	
	14 → 13	23.8	

Table III: GaAs channeling-radiation transition energies for 54.4-MeV positrons.

Plane	Transitions	Calculated energy	Measured energy
(100)	13 → 10	64.1	
	11 → 8	60.8	
	10 → 9	59.3	
	9 → 6	58.1	Peak at
	12 → 11	58.1	54.1 ± 0.5 keV
	8 → 7	57.8	
	7 → 4	54.7	FWHM
	6 → 5	54.7	12.9 ± 1 keV
	5 → 2	51.1	
	4 → 3	51.1	
	3 → 0	46.8	
	2 → 1	46.8	
(110)	12 → 11	56.2	
	11 → 10	55.1	
	10 → 9	53.6	
	9 → 8	51.8	Peak at
	8 → 7	49.9	43.4 ± 0.4 keV
	7 → 6	47.8	
	6 → 5	45.7	FWHM
	5 → 4	43.5	16.3 ± 1 keV
	4 → 3	41.3	
	3 → 2	39.4	
	2 → 1	38.0	
	1 → 0	37.3	

Figure Captions

Fig. 1 GaAs planar potentials and eigenvalues for 16.9-MeV (γ = 34.0) electrons for
a) the (100) plane;
b) the (110) plane; and
c) the (111) plane.

Fig. 2 GaAs channeling-radiation spectra for 16.9-MeV (γ = 34.0) electrons for
a) the (100) plane;
b) the (110) plane; and
c) the (111) plane.

Fig. 3 GaAs planar potentials and eigenvalues for 54.4-MeV (γ = 107.5) electrons for
a) the (100) plane;
b) the (110) plane; and
c) the (111) plane.

Fig. 4 GaAs channeling-radiation spectra for 54.4-MeV (γ = 107.5) electrons for
a) the (100) plane;
b) the (110) plane; and
c) the (111) plane.

Fig. 5 GaAs planar potentials and eigenvalues for 54.4-MeV (γ = 107.5) positrons for
a) the (100) plane; and
b) the (110) plane.

Fig. 6 GaAs channeling-radiation spectra for 54.4-MeV (γ = 107.5) positrons for
a) the (100) plane; and
b) the (110) plane.

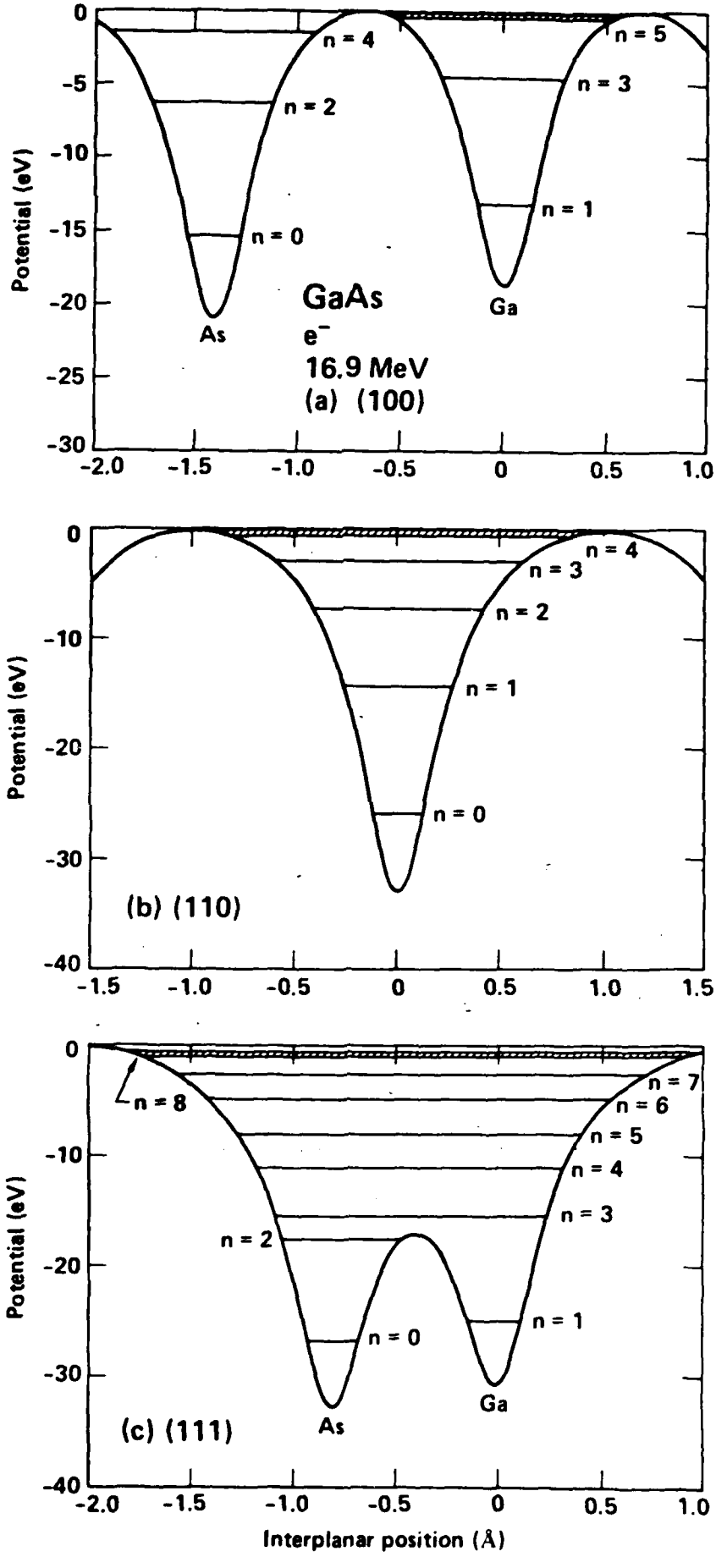
Potential (eV)
0
-5
-10
-15
-20
-25
-30
-2.0
-1.5
-1.0
-0.5
0
0.5
1.0
n = 4
n = 5
n = 3
n = 2
n = 1
n = 0
As
Ga
GaAs
e⁻
16.9 MeV
(a) (100)
-40
1.5
(b) (110)
n = 7
n = 6
n = 8
n = 5
n = 4
n = 3
n = 2
n = 1
n = 0
(c) (111)
Interplanar position (Å)

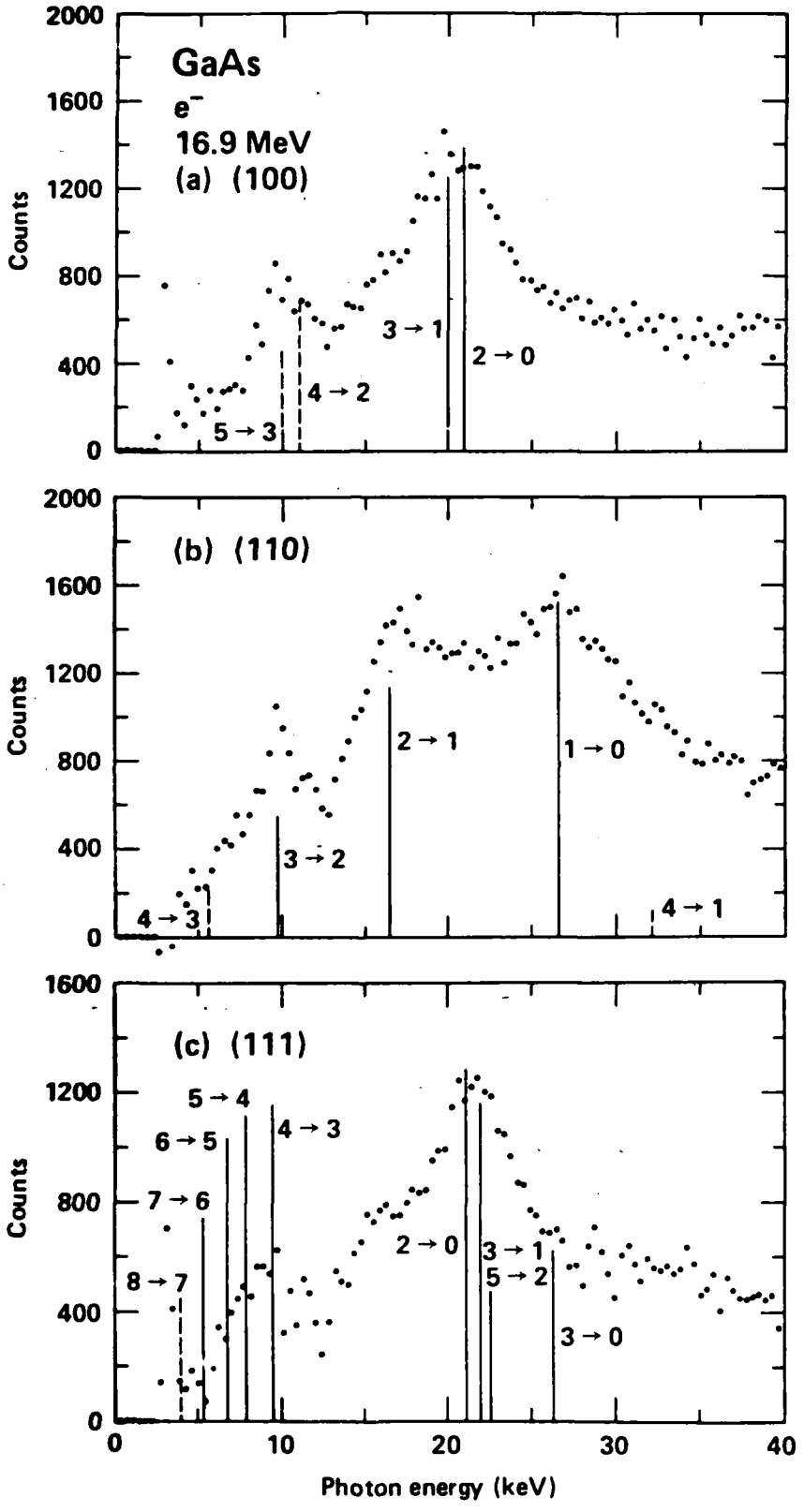
GaAs
e⁻
16.9 MeV
(a) (100)
5 → 3
4 → 2
3 → 1
2 → 0
(b) (110)
4 → 3
3 → 2
2 → 1
1 → 0
4 → 1
(c) (111)
8 → 7
7 → 6
6 → 5
5 → 4
4 → 3
2 → 0
3 → 1
5 → 2
3 → 0
Counts
Photon energy (keV)
0
400
800
1200
1600
2000
10
20
30
40

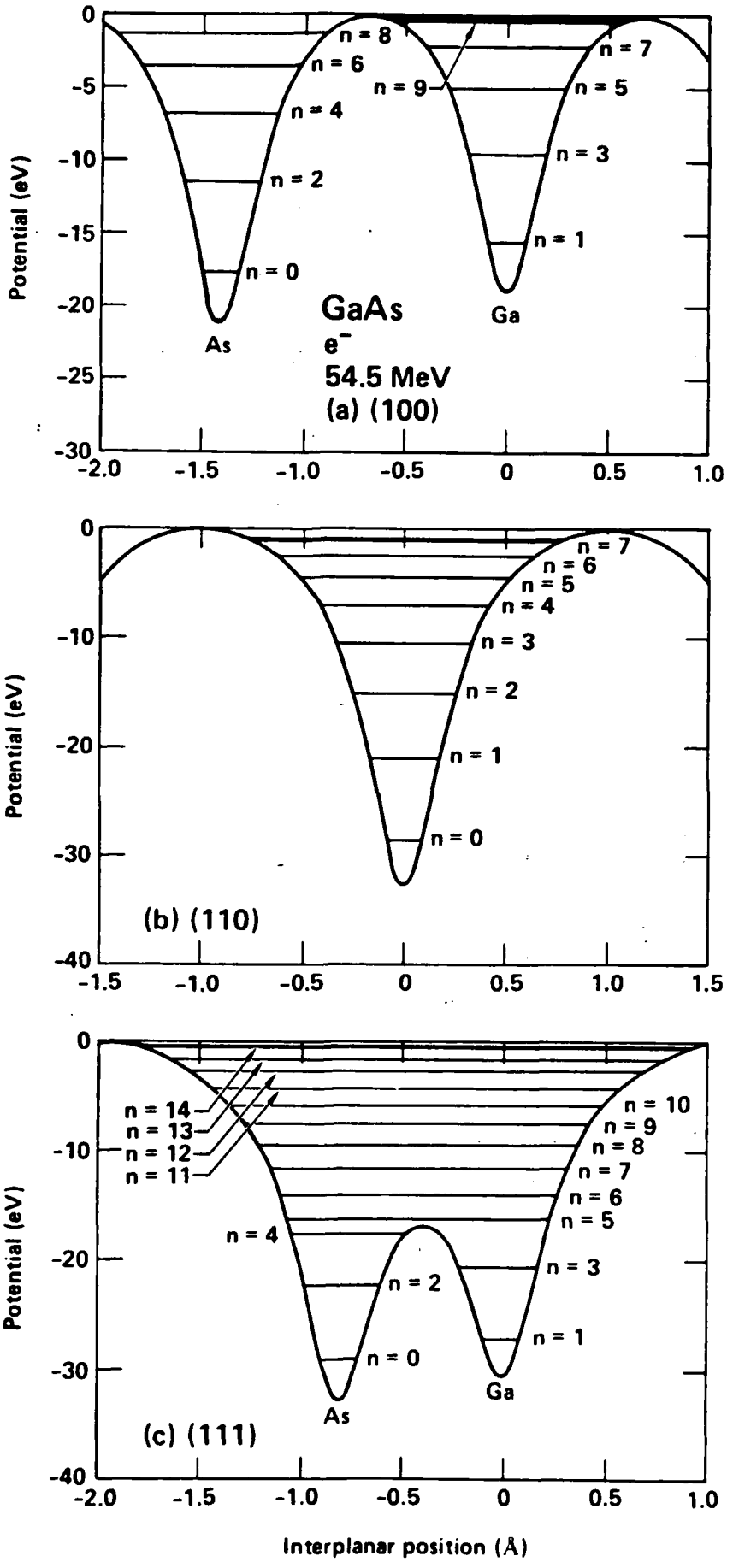
Potential (eV)
0
-5
-10
-15
-20
-25
-30
-2.0
-1.5
-1.0
-0.5
0
0.5
1.0
n = 8
n = 6
n = 4
n = 2
n = 0
n = 9
n = 7
n = 5
n = 3
n = 1
As
Ga
GaAs
e⁻
54.5 MeV
(a) (100)
-40
1.5
(b) (110)
n = 14
n = 13
n = 12
n = 11
n = 10
(c) (111)
Interplanar position (Å)

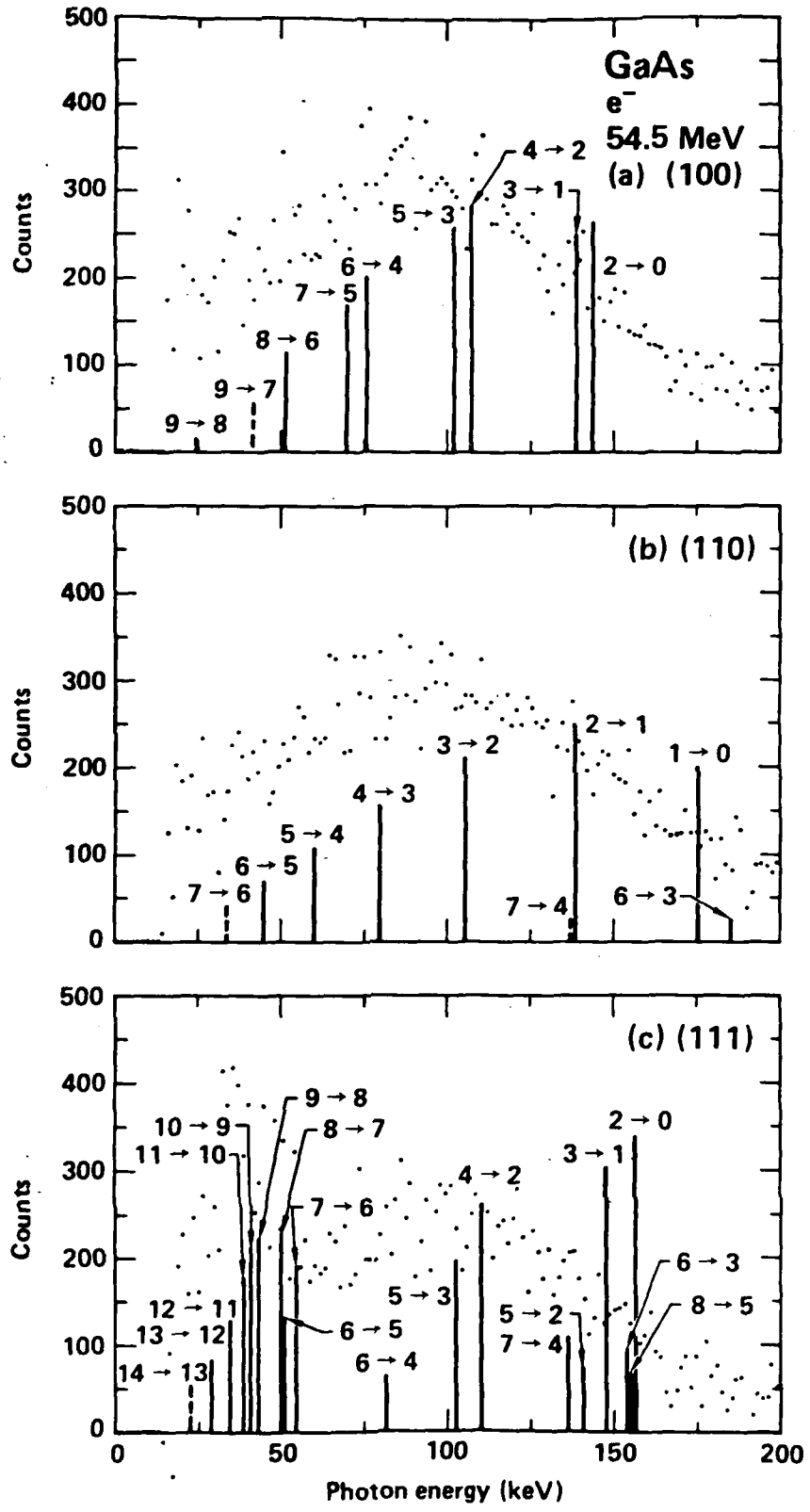
GaAs
e⁻
54.5 MeV
(a) (100)
(b) (110)
(c) (111)
Counts
Photon energy (keV)
0
50
100
150
200
100
200
300
400
500
9 → 8
9 → 7
8 → 6
7 → 5
6 → 4
5 → 3
4 → 2
3 → 1
2 → 0
7 → 6
6 → 5
5 → 4
4 → 3
3 → 2
2 → 1
1 → 0
7 → 4
6 → 3
14 → 13
13 → 12
12 → 11
11 → 10
10 → 9
9 → 8
8 → 7
7 → 6
6 → 5
6 → 4
5 → 3
5 → 2
4 → 2
3 → 1
2 → 0
7 → 4
6 → 3
8 → 5

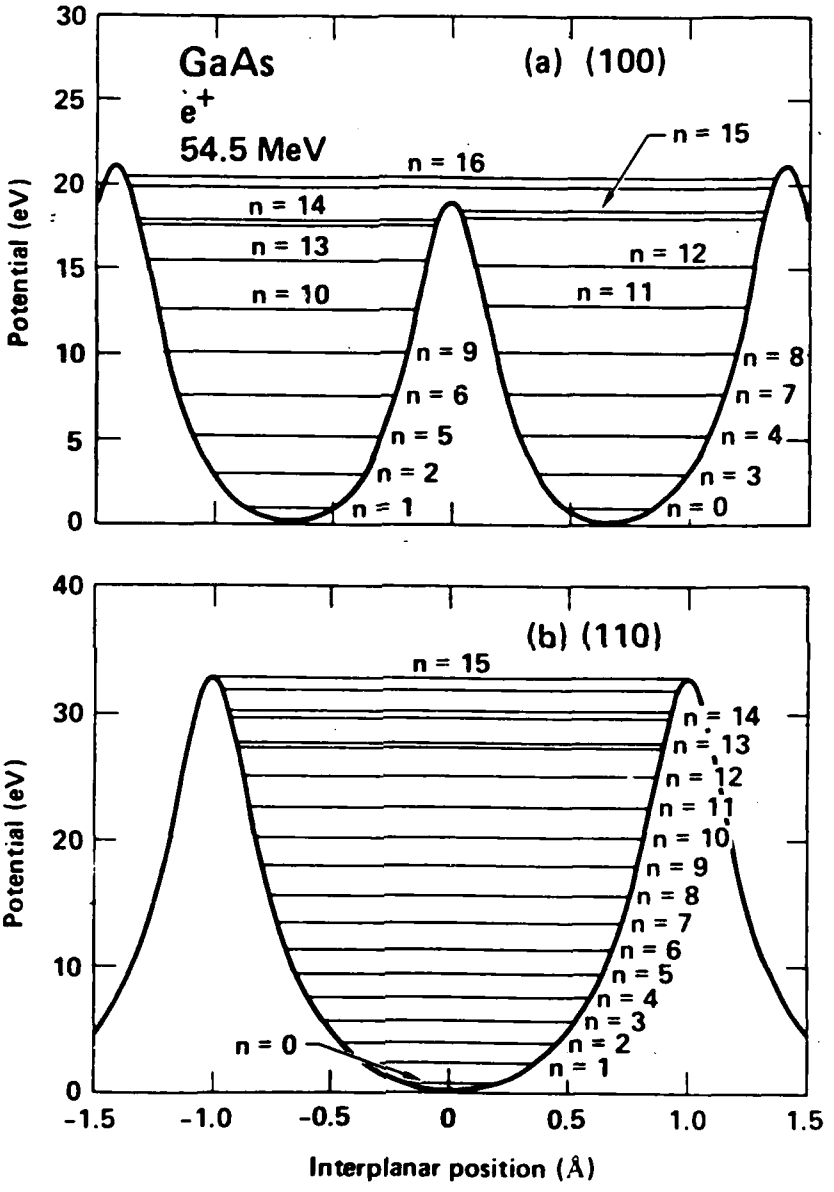
GaAs
e+
54.5 MeV
(a) (100)
n = 16
n = 15
n = 14
n = 13
n = 12
n = 11
n = 10
n = 9
n = 8
n = 7
n = 6
n = 5
n = 4
n = 3
n = 2
n = 1
n = 0
Potential (eV)
(b) (110)
n = 15
n = 14
n = 13
n = 12
n = 11
n = 10
n = 9
n = 8
n = 7
n = 6
n = 5
n = 4
n = 3
n = 2
n = 1
n = 0
Potential (eV)
Interplanar position (Å)

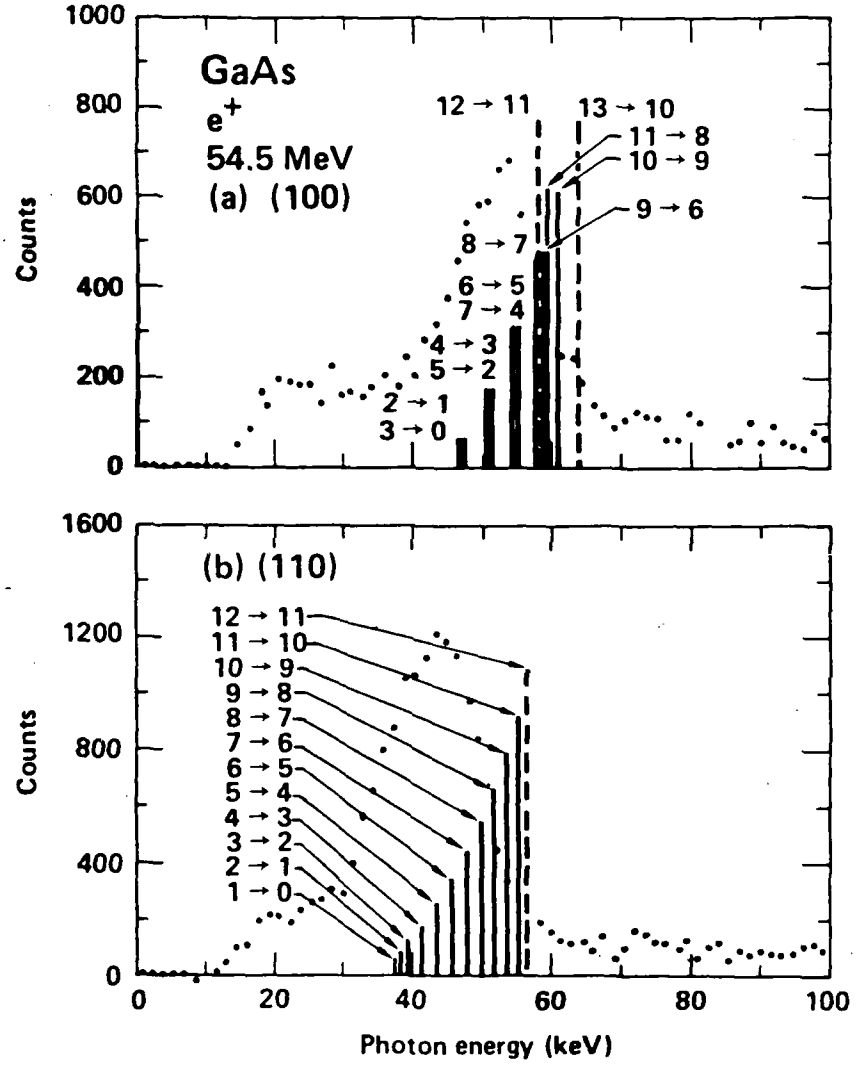
GaAs
e+
54.5 MeV
(a) (100)
12 → 11
13 → 10
11 → 8
10 → 9
9 → 6
8 → 7
6 → 5
7 → 4
4 → 3
5 → 2
2 → 1
3 → 0
(b) (110)
12 → 11
11 → 10
10 → 9
9 → 8
8 → 7
7 → 6
6 → 5
5 → 4
4 → 3
3 → 2
2 → 1
1 → 0
Counts
Counts
Photon energy (keV)
0
200
400
600
800
1000
1200
1600
20
40
60
80
100

Electron channeling radiation from diamonds with and without platelets

H. Park, J. O. Kephart, R. K. Klein, and R. H. Pantell
Department of Electrical Engineering, Stanford University, Stanford, California 94305

B. L. Berman
Lawrence Livermore National Laboratory, University of California, Livermore, California 94550 and Department of Physics, George Washington University, Washington, D. C. 20052

S. Datz
Oak Ridge National Laboratory, Oak Ridge, Tennessee 37830

R. L. Swent
Varian Associates, Palo Alto, California 94303

(Received 24 July 1984; accepted for publication 16 October 1984)

Channeling-radiation spectra produced by planar-channeled, 30.5-MeV electrons in Type-Ia and Type-IIa natural diamonds have been measured and are compared with previous results for 54.5-MeV electrons. Because of the presence of platelets precipitated along the (100) planes in the Type-Ia diamond, the energies of the (100) spectral peaks are shifted downward relative to those for the Type-IIa diamond. We have developed a model to explain this effect.

I. INTRODUCTION

In a previous paper[1] we presented experimental data for the channeling radiation produced by 54.5-MeV electrons and positrons in Type-Ia and Type-IIa natural diamonds. Type-Ia diamonds contain platelets precipitated along the (100) planes; Type-IIa diamonds do not. For both electrons and positrons, the spectral features (peak energies, linewidths, and intensities) of the two types were different. Perhaps the most interesting feature is the downshift in energy of the spectral peaks for electrons incident along the (100) plane in the Type-Ia diamond relative to those for the Type-IIa diamond. In this paper we present a model to explain this observation, along with additional data obtained for 30.5-MeV channeled electrons.[2]

More extensive measurements on the Type-IIa diamond have been presented and discussed in detail in Ref. 3. The first channeling-radiation data reported for diamond in this energy range were obtained at Saclay using a nearly defect-free portion of a synthetic diamond.[4]

Ninety-eight percent of all natural diamonds are of Type Ia and only about 1% are of Type IIa. Type-Ia diamonds contain platelets, which apparently are interplanar aggregates of atoms, at least partly nitrogen, precipitated during the cooling phase of their growth along (100) planes in single or double layers. Evans[5] summarized the properties of platelets as they were known in 1976. Models of platelets as (a) double layers of predominantly nitrogen atoms or (b) single layers of predominantly carbon (but possibly nitrogen) atoms have been proposed by Lang[6] and Humble,[7] respectively. Barry *et al.*[8] have proposed a new "zig-zag" model, which is similar to the Lang model in its use of double layers of nitrogen atoms but is different in the details of their structure and spacing. A recent measurement[9] using high-resolution electron energy-loss spectroscopy has shown conclusively that nitrogen is a major constituent of platelets. Of greater significance to the present work, however, is the displacement of the (100) planes which results from the presence of a platelet. The Lang model, pictured in Fig. 1(a), gives a total displacement of $a/3$, where $a = 3.567$ Å is the lattice constant for diamond. The Humble model, pictured in Fig. 1(b), gives a total displacement of $0.4a$. More recent analyses have yielded values of $0.35a$ (Ref. 10) and $(0.33 \pm 0.05)a$ (Ref. 11). Further details of the related structural properties of diamonds can be found in Refs. 12 and 13.

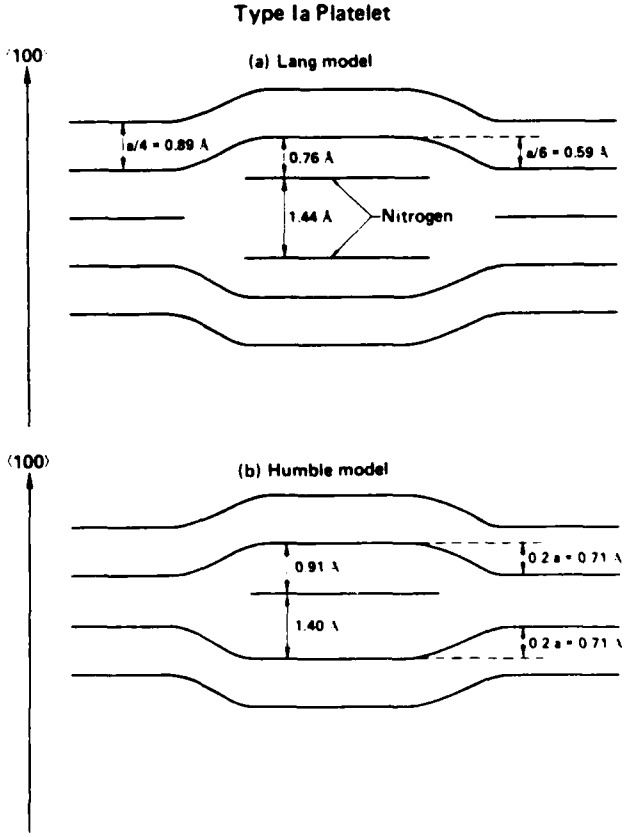

FIG. 1. Schematic representations of a platelet in a Type -Ia diamond crystal: (a) according to the model of Lang (Ref. 6), the platelet consists of a double layer of nitrogen atoms; (b) according to the model of Humble (Ref. 7), it consists of a single layer of carbon (or possibly nitrogen) atoms.

 0021-8979/85/051661-04$02.40

Along the (111) planes, the platelets disrupt the crystal structure in much the same way as do stacking faults, displacing the planes by a distance equal to $1/\sqrt{3}$ of the displacement of the (100) planes. A similar situation pertains to the (110) planes, except that for this case the displacement is equal to $1/\sqrt{2}$ of the displacement of the (100) planes. Along the (100) planes, on the other hand, it can be seen from Fig. 1 that the platelets cause a distortion (rather than a disruption) of the crystal structure.

II. EXPERIMENTAL RESULTS

The experiment was performed with a 30.5-MeV electron beam from the Lawrence Livermore National Laboratory Electron-Positron Linear Accelerator. A comprehensive summary of the details of the experimental apparatus and techniques, together with the details of the calculational methods we use to compare theoretical and experimental results, is given in Ref. 3.

The 12-μm-thick Type-Ia diamond was cut normal to its ⟨110⟩ axis, and the 23-μm-thick Type-IIa diamond was cut normal to its ⟨100⟩ axis. Transmission-electron-microscopy photographs of the Type-Ia diamond showed platelet diameters that varies from 40 Å to over 200 Å, with an average separation of $\sim$500 Å. From an infrared-absorption measurement, we estimate (see Ref. 13) that the mean separation between platelet encounters for a planar-channeled electron is $\sim$4500 Å.

The radiation spectra from 30.5-MeV electrons channeled along the three major planes of diamond are shown in Fig. 2. These results were obtained by subtracting the bremsstrahlung spectra produced when the orientation of the crystal was in a random direction relative to the electron-beam direction from those when it was aligned along a major crystal plane. In each part of the figure, two spectra are superposed, corresponding to the two diamonds used. These two spectra were normalized to each other by matching the photon yields in the 500–700-keV photon-energy region.

The parameters of the spectral peaks are listed in Table I. For the (111) plane [Fig. 2(a)], the effect of the platelets is a modest decrease in intensity, whereas for the (110) plane [Fig. 2(b)], the reduction in intensity caused by the platelets is so severe that no individual spectral lines can be discerned. Both of these effects can be explained in terms of the heuristic model of Ref. 1. The density of platelets is such that a channeled electron encounters $\sim$25 platelets in traversing the 12-μm-thick Type-Ia diamond. In the (111) direction, the

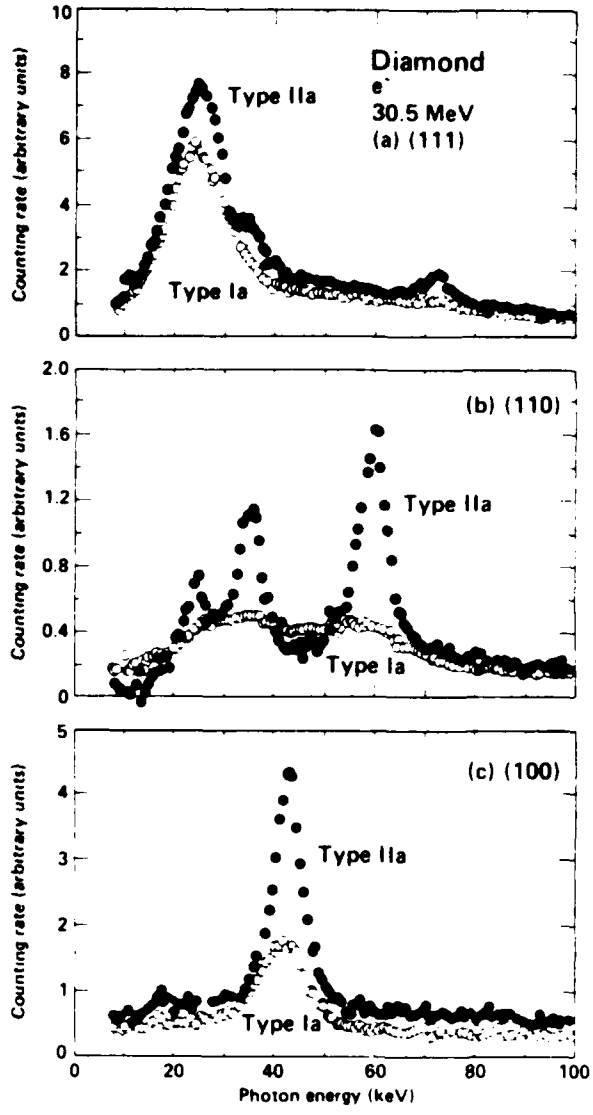

FIG. 2. Channeling-radiation spectra from both Type-Ia (open data points) and Type-IIa (closed data points) diamonds, for 30.5-MeV electrons incident along (a) the (111) planar direction, (b) the (110) planar direction, and (c) the (100) planar direction.

dechanneling probability of an electron in crossing a stacking fault is $<1\%$ because of the alternating wide and narrow spacings of the planes (see Ref. 1), whereas in the (110) direction, it is $>15\%$ because there is no such alternation. After

TABLE I. Measured characteristics of 30.5-MeV electron channeling radiation from diamond crystals

Plane	Transition	Type IIa (without platelets)			Type Ia (with platelets)		
		Peak energy (keV)	Relative intensity	Width (keV)	Peak energy (keV)	Relative intensity	Width (keV)
(111)	Several	25.0 ± 0.5	1.88	11.8 ± 0.8	24.2 ± 0.6	1.27	13.3 ± 1.3
(110)	1→0	60.1 ± 0.3	1.07	6.0 ± 0.3			
	2→1	35.3 ± 0.3	0.62	5.2 ± 0.3	No discernible line radiation		
	3→2	24.5 ± 0.2	0.28	4.8 ± 0.3			
(100)	1→0	43.0 ± 0.3	1.00	5.9 ± 0.3	41.3 ± 0.4	0.38	10.8 ± 1

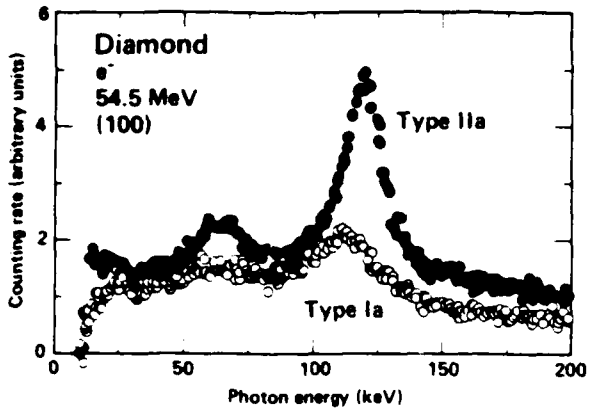

FIG. 3. Channeling-radiation spectra from Type-Ia (open data points) and Type-IIa (closed data points) diamonds, for 54.5-MeV electrons incident along the (100) planar direction.

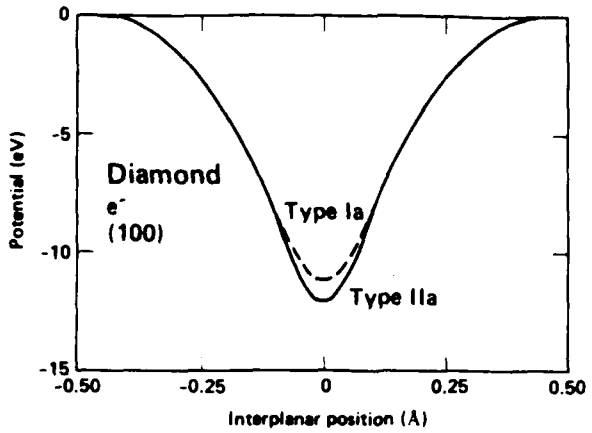

FIG. 4. Potentials for the (100) plane in diamond. The solid curve represents the potential which uses the accepted value of 0.040 Å for the thermal-vibration amplitude, as is appropriate for Type-IIa diamonds. The dashed curve represents the potential which uses the value of 0.055 Å, which arises from a best fit to the data for the Type-Ia diamond of the present experiment.

~25 such crossings, the (111) intensity would be reduced by ~20%, while the (110) intensity would be reduced to virtually nothing.

For the (100) plane, we show the 54.5-MeV data from Ref. 1 in Fig. 3, as well as the present 30.5-MeV data in Fig. 2(c). Here we see a reduction in intensity by a factor of ~2.5, corresponding to a dechanneling probability of ~3.5% per platelet encounter. More importantly, we observe a downshift in energy of the 1→0 spectral peak of about 4% for 30.5-MeV electrons and about 8% for 54.5-MeV electrons. For the 54.5-MeV case, the downshift of the 2→1 peak is about 3%; this transition is not observable at 30.5 MeV because the $n = 2$ state is not bound for this case.

III. THEORETICAL MODEL

The inclusion of atomic thermal vibrations in the derivation of crystalline potentials results in an energy downshift for the deeply-bound states. We have observed this same effect, i.e., an energy downshift, when platelets are introduced into the crystal, which suggests that platelets are similar to thermal vibrations in that they cause an uncertainty in the position of the atoms. Therefore, in our model, to explain the data we assume an effective vibrational amplitude that is the quadrature sum of the actual amplitude and a displacement resulting from the presence of the platelets.

In calculating the theoretical transition energies, we employ the Hartree–Fock potential, modified by a Debye–Waller factor to account for thermal vibrations (see Ref. 3 for the details of how this is done). For the Type-IIa diamond (without platelets), we use the tabulated[14] thermal-vibration amplitude of 0.04 Å. The (100) planar potential so derived is shown as the solid curve in Fig. 4, from which one obtains the calculated transition energies listed in column 3 of Table II. These values agree very well with the measured (100) transition energies for the Type-IIa diamond listed in column 4 of the table.

The measured (100) transition energies for the Type-Ia diamond, listed in column 5 of Table II, are lower (by 3 to 9%) than the calculated values which use the above value for the thermal-vibration amplitude. When we allow this amplitude to vary, a best fit to the data is achieved for a value of 0.055 Å. This new value produces the calculated (100) transition energies listed in the last column of Table II and corresponds to the (100) potential shown as the dashed curve in Fig. 4. This result implies that the platelets contribute an equivalent vibrational amplitude of 0.038 Å.

In the preceding derivation, we assumed that the platelets introduced a probability density function for the position of the atoms given by a Gaussian distribution with a standard deviation equal to 0.038 Å. We attempted to use other probability density functions (a uniform distribution and a discrete distribution) as well, but we were unable to match the data. This suggests that the Gaussian function is appropriate.

TABLE II. Transition energies (in keV) for (100) planes in diamond.

Electron energy (MeV)	Transition	Calculated with standard potential	Measured		Calculated with modified potential
			Type IIa		Type Ia
30.5	1→0	43	43.0 ± 0.3[a]	41.3 ± 0.4	41
54.5	1→0	122	119.8 ± 0.7[a]	111.0 ± 2	113
	2→1	65	64.7 ± 1.5[a]	~63	63

[a] These values supersede the (slightly different) values given in Ref. 1.

How reasonable is the 0.038 Å displacement that was calculated? We estimate an average platelet diameter of about 140 Å and a distance of about 4500 Å between platelet encounters along a major plane. This gives a mean displacement of the (100) planes of 0.037 Å for the Lang model and 0.044 Å for the Humble model. These rough calculations indicate that the calculated displacement of 0.038 Å is not unreasonable and thus that the analysis of channeling-radiation data may lead to a better understanding of the structure of these kinds of aggregate impurities or defects in crystals.

Finally, a comparison can be made between the coherence lengths in the crystal, as obtained from the observed linewidths of the spectral peaks and the mean distance between platelets determined from infrared-absorption measurements. Assuming a Lorentzian line shape, the full width half maximum (FWHM) linewidth ΔE is related to the coherence length $l_{\rm coh}$ by the relationship $l_{\rm coh} = 2\gamma^2\hbar c/\Delta E$.

This comparison is applicable only for the $1\rightarrow 0$ transition for (100) planes, since this is the only transition for which the spectral peak is not overlapped by other transitions and stands sufficiently above the background to provide an accurate measure of the linewidth. The coherence length is found to be 0.13 μm at a beam energy of 30.5 MeV and 0.17 μm at a beam energy of 54.5 MeV.

The infrared-absorption data indicate a mean separation between platelets of 0.45 μm. If this is taken to be the coherence length for both the $n = 0$ and $n = 1$ states, then the coherence length for the $1\rightarrow 0$ transition is calculated to be 0.22 μm. However, there are other line-broadening mechanisms which tend to reduce $l_{\rm coh}$. The most important of these arises from the thermal vibrations of the atoms; including this effect, the coherence length becomes 0.18 μm. This calculated value is in reasonable agreement with the values obtained from the measured spectral linewidths.

ACKNOWLEDGMENTS

The authors are grateful to Professor J. P. F. Sellschop for providing the Type-IIa diamond and to Dr. R. W. Fearick for several valuable discussions. This work was performed at Lawrence Livermore National Laboratory under the auspices of the U.S. Department of Energy under Contract No. W-7405-ENG-48 and was supported as well by the U. S. Air Force Office of Scientific Research under Grant No. AFOSR-81-0209, by the U. S. Joint Services Electronics Program under Grant No. DAAG-29-81-K-0057, by the National Science Foundation under Grant No. ECS-18139, and by the U. S. Department of Energy under Contract No. W-7405-ENG-26.

[1] H. Park, R. H. Pantell, R. L. Swent, J. O. Kephart, B. L. Berman, S. Datz, and R. W. Fearick, J. Appl. Phys. **55**, 358 (1984).

[2] A preliminary version of these data has been presented in S. Datz, R. W. Fearick, H. Park, R. H. Pantell, R. L. Swent, J. O. Kephart, and B. L. Berman, Nucl. Instrum. Methods **B 2**, 74 (1984).

[3] R. K. Klein, J. O. Kephart, R. H. Pantell, H. Park, B. L. Berman, R. L. Swent, S. Datz, and R. W. Fearick, Phys. Rev. B (in press); see also S. Datz, R. W. Fearick, H. Park, R. H. Pantell, R. L. Swent, J. O. Kephart, R. K. Klein, and B. L. Berman, Phys. Lett. A 96, 314 (1983).

[4] M. Gouanère, D. Sillou, M. Spighel, N. Cue, M. J. Gaillard, R. G. Kirsch, J.-C. Poizat, J. Remillieux, B. L. Berman, P. Catillon, L. Roussel, and G. M. Temmer, Nucl. Instrum. Methods **194**, 225 (1982).

[5] T. Evans, Contemp. Phys. **17**, 45 (1976).

[6] A. R. Lang, Proc. Phys. Soc. London **84**, 871 (1964).

[7] P. Humble, Proc. R. Soc. London Ser. A **381**, 65 (1982).

[8] J. C. Barry, L. A. Bursill, and J. L. Hutchison, Philos. Mag. (in press). We thank Prof. J. Spence for bringing this latest work to our attention.

[9] S. J. Pennycook, Bull. Am. Phys. Soc. **28**, 1318 (1983).

[10] L. A. Bursill, J. L. Hutchison, A. R. Lang, and N. Sumida, Nature (London) **292**, 518 (1981).

[11] J. C. Barry, L. A. Bursill, and J. L. Hutchison, Philos. Mag. A **48**, 109 (1983).

[12] G. Davies, Chem. Phys. Carbon **13**, 1 (1977).

[13] R. W. Fearick and J. P. F. Sellschop, Nucl. Instrum. Methods **168**, 195 (1980).

[14] D. S. Gemmell, Rev. Mod. Phys. **46**, 129 (1974).

Novel Radiation Sources for Infrared to Gamma Rays

R.H. Pantell

Department of Electrical Engineering
Stanford University
Stanford, CA 94305

There are a variety of methods for generating radiation in the range from infrared to gamma rays, and four different techniques using charged particle beams will be presented. The first three are considered as spontaneous emissions sources, and the last as a stimulated source. None of the approaches are likely to be suitable for insertion in a storage ring, since they all involve a significant alteration in particle trajectories.

1. Transition radiation.

Transition radiation occurs when a moving, charged particle encounters an interface across which there is a change in permittivity.[1-3] For example, in moving from vacuum into a metal an electron establishes image charges in the metal giving rise to dipole emission. Dipole radiation is zero in the direction of motion, and for a relativisitic particle characterized by γ, where γ is the ratio of particle energy to its rest energy, the angle θ for maximum intensity is $\theta = \gamma^{-1}$. The emission cone is illustrated in Figure 1.

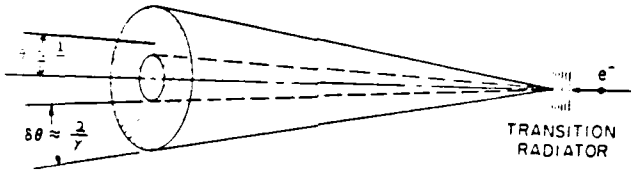

Figure 1. The transition radiation cone for an electron passing through a stack of foils. Maximum intensity is for $\theta = \gamma^{-1}$ with a cone width $\delta\theta = 2\gamma^{-1}$

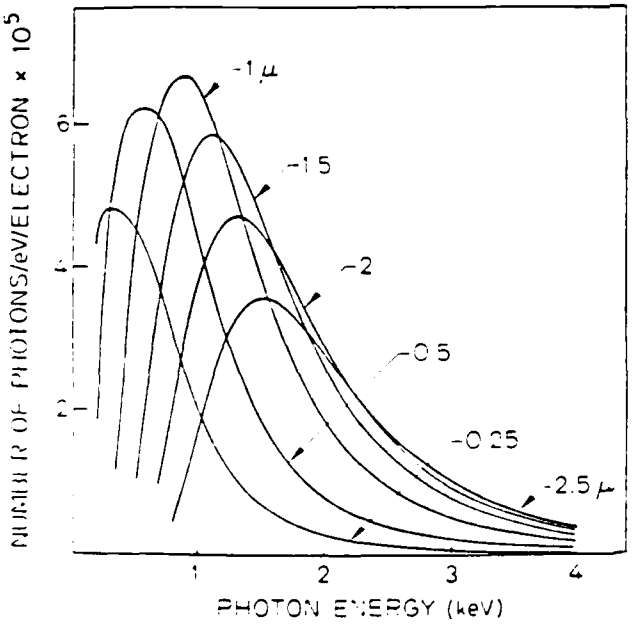

The emission spectrum is given approximately by the transform of a pulse in time, with a reduction at low photon energies because of material absorption. Figure 2 shows the calculated emission from a stack of 25 Be foils for an electron energy of 100 MeV. The peak is shifted to higher photon energies for thicker foils because of reabsorption in the Be. Maximum intensity occurs for a thickness of 1.0μ, which corresponds to the length (for the selected parameter values) for which the electron slips π radians in the phase of an electromagnetic wave within the foil. This is the maximum distance over which the particle can radiate into a fixed sign of the field.

Figure 2. Theoretically predicted emission from 25 foils of various thicknesses of Be for an electron energy of 100 MeV.

There is excellent agreement between theory and experiment, as shown in Figure 3.[4] Figure 3a illustrates the calculated (solid line) and measured spectra (dots) from 54 MeV electrons, without any scale adjustments, for 18 Be foils, each 1.0μ thick, and separated by 1.5 mm. Figure 3b is for 30 Al foils with the same thickness and separation.

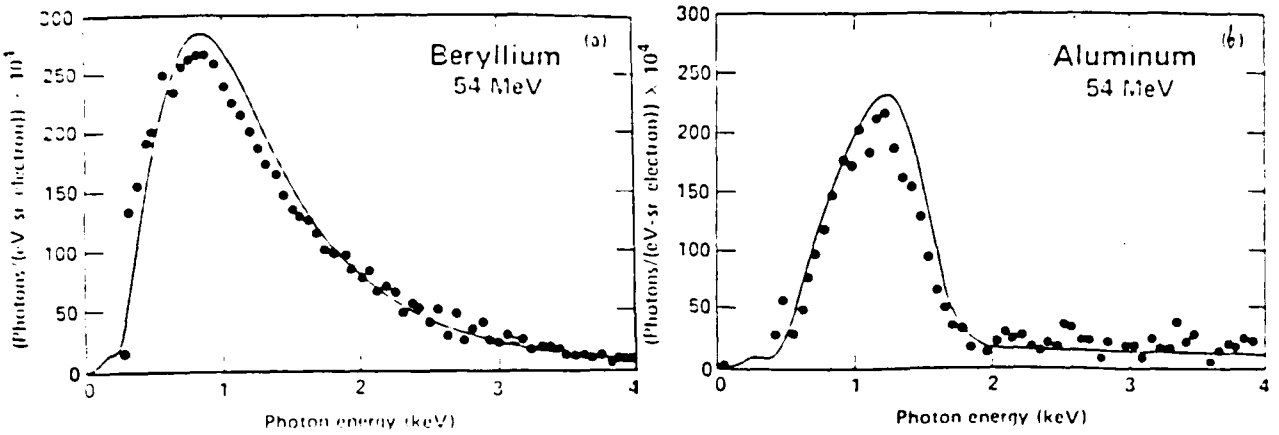

Figure 3. Emission from 54 MeV electrons passing through:
(a) Eighteen Be foils, each 1.0μ thick and separated by 1.5 mm.
(b) Thirty Al foils, each 1.0μ thick and separated by 1.5 mm.

The intensity of emission depends upon the foil material, diameter, thickness and separation; upon γ; and upon the beam current. Figure 4 illustrates the parameters that will produce 25mW of power from a Be foil stack over a half-maximum bandwidth of ±50%. The length of the stack is one meter and the foil diameter is 1.0mm,[5] and the foil thickness and separation between foils have been chosen to maximize power.[5] In terms of photon flux, 25mW corresponds to 10^{14} photons per second for $\hbar\omega$ = 1.6keV. At the current levels shown in Figure 4, it would be necessary to circulate a coolant, such as H_2 gas, between the foils to avoid excessive heating.

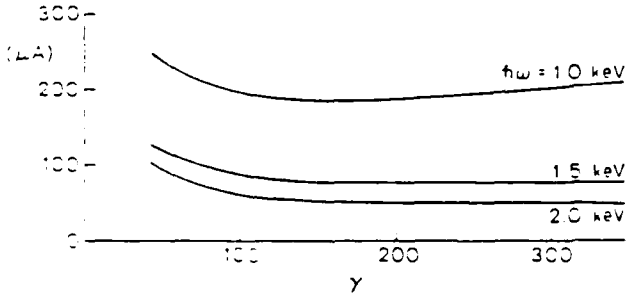

Figure 4. The current required to produce 25 mW of power by transition radiation from a stack of Be foils as a function of particle energy. The foils are spaced to maximize emission per unit length. Each curve is for a different mean photon energy and a half-maximum bandwidth of ± 50% is assumed.

2. Channeling radiation.

Charged particles moving through a crystal can be trapped in the potential well between planes or along axes. This effect, known as channeling, causes the particle to move in a periodic trajectory and to emit radiation at a wavelength determined by the periodicity of the motion, the energy of the particle, and the direction of observation.[6]

An x-ray and γ-ray source obtained from channeling radiation has a number of interesting properties: it occurs in a narrow emission cone with a cone half-angle equal to γ^{-1}; the emission is linearly polarized; spectral peaks are generated with linewidths that range from 10-25%; the location of the peaks can be adjusted by altering the beam energy or the crystal material; the emitted photon flux is ≈ 10^{11} photons per second in 10% bandwidth; and the time structure of the emission reproduces that of the particle beam, giving pulses of radiation that are several picoseconds long.

From a quantum viewpoint, the particle is trapped in a potential well and emission results from spontaneous transitions between eigenstates. Figure 5 shows the potential function for positrons channeled by (110) planes in Si, as obtained from a Hartree-Fock model. The abscissa is the distance in Å between adjacent planes, where x = 0 is the midpoint. The corresponding eigenvalues, calculated by substituting a summation of Bloch waves into the wave equation, are for $\gamma = 107$. Radiation results primarily from $\Delta n = 1$ transitions, although $\Delta n = 3$ transitions have also been observed. In the direction of relativistic motion, the emitted photon energy equals $2\gamma^2(\Delta E)$, where ΔE = energy difference between eigenstates.

Figure 6 shows the emission from the positrons, with the spectral peak at ≈ 40 keV energy corresponding to the $\Delta n = 1$ transitions in Figure 5. The line below this peak is the bremsstrahlung background, obtained by orienting the crystal in a random direction.

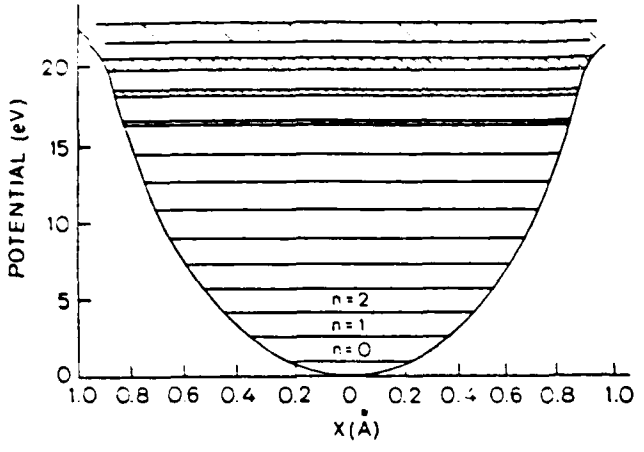

Figure 5. The potential function for positrons channeled by (110) planes in Si as a function of the distance between planes. (x = 0 corresponds to the midpoint.) Eigenvalues are for $\gamma = 107$ particles, and radiation results from spontaneous transitions between eigenstates.

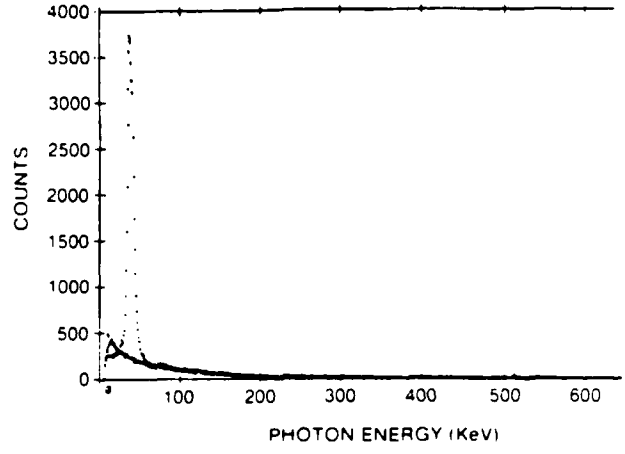

Figure 6. Channeling radiation as a function of photon energy for $\gamma = 107$ positrons channeled by (110) planes in Si.

Planar channeling radiation has been observed in a variety of crystals,[7-9] and Table I lists the measured photons per micron of crystal length per particle, for $\gamma = 107$ electrons and positrons in different materials. For positrons, the radiation has been integrated over the photon energy range from 20 to 70 keV, and for electrons the range is from > 0 to 150 keV. From this table it is seen that photon emission per unit length increases with Z, the average atomic number for the crystal. However, the length for which the particle remains channeled has yet to be determined for most crystals, and so the total emission is not known.

Table I

Channeling Radiation (photons/μm per particle radiated into a detector with a solid angle acceptance of 50×10^{-6} ster) from 54 MeV Planar-Channeled Electrons and Positrons.

Crystal	Z	Electron	Positron	Error
LiH	2	0.6×10^{-8}	1.2×10^{-8}	± 30%
Be	4	1.5×10^{-8}	---	± 10%
C	6	7.6×10^{-8}	1.0×10^{-7}	± 20%
LiF	6	1.9×10^{-7}	1.5×10^{-7}	± 10%
Si	14	8.3×10^{-7}	8.6×10^{-7}	± 10%
Ge	32	8.0×10^{-7}	2.0×10^{-7}	± 30%
W	74	8.4×10^{-6}	1.3×10^{-5}	± 50%

As an example of emission intensity, consider γ = 100 electrons planar channeled in a 100μ thick Be crystal. (100μ is an approximate value for the channeling length.) The average current that can flow through the crystal is limited by heating and defect formation, and for a 1.0 cm^2 beam area this is = 100 μA. For this current, $\sim 10^{11}$ photons/sec. are emitted in 10% bandwidth at a wavelength of 0.1Å into a cone with a 10 mrad half-angle. By increasing γ to ~2000, gamma rays have been generated[10,11] at a wavelength of $\lambda = 10^{-3}$Å.

3. X-ray Cherenkov radiation.

Cherenkov radiation occurs when the velocity of a charged particle in a medium exceeds the velocity of light in that medium. This requires an index of refraction, n, greater than unity, and in the x-ray portion of the spectrum, except near an absorption edge,

$$n = 1 - \frac{1}{2}\left(\frac{\omega_p}{\omega}\right)^2 \qquad (1)$$

where ω_p is the plasma frequency of the medium. However, close to an absorption, such as a K or L-shell transition, n can become greater than unity, thereby allowing Cherenkov emission.

The radiation is in the form of a cone, as shown in Figure 7, where the cone angle θ_c is given by

$$\theta_c^2 = 2(n-1) - \frac{1}{\gamma^2} \qquad (2)$$

and the field vector is polarized along the radial direction.

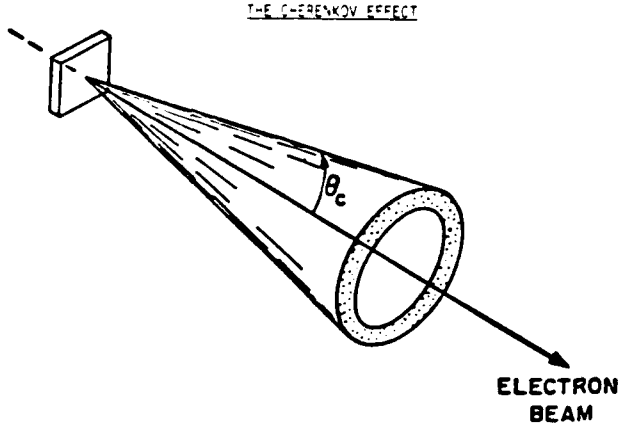

Figure 7. The Cherenkov Radiation is in a cone centered about the direction of particle motion, with a cone angle θ_c given by $\theta_c = \cos^{-1}(\beta n)^{-1}$.

Table II lists the maximum values for (n-1) that occur in several different materials near K or L-shell absorption edges. These numbers were calculated from the absorption curves, using the Kramers-Kronig integral and subtracting the plasma contribution to permittivity. For graphite the Cherenkov radiation has been measured,[12] and the value for (n-1) corresponding to the observed emission angle agrees quite well with the calculated (n-1). All the materials listed in Table II should emit Cherenkov x-rays at the designated wavelengths.

Table II

Values for (n-1) for several different materials near absorption edges.

		$10^3 \times (n-1)_{MAX}$	
Element	λ(Å)	Calculated	Measured
Be (K-shell)	112	68	
Graphite (K)	43.7	7.4	6.8
Diamond (K)	43.7	11.4	
Ti (L)	27.2	4.7	
Al (K)	7.9	0.1	

X-ray Cherenkov emission is a fixed-wavelength source, obtainable with relatively low γ particles, which can provide quite relatively high flux rates. For example, consider the carbon K shell absorption at λ = 43Å ($\hbar\omega$ = 284 eV). Photons emitted per unit frequency $dN/d\omega$ is given by

$$\frac{dN}{d\omega} = \frac{\alpha l}{c} \sin^2\theta_c \qquad (3)$$

where α = 1/137 and l = interaction length. Using a stack of 100 foils, each 2μ thick, a beam current of 150 μA at γ = 20 gives a flux rate of 10^{14} photons/sec in 0.5% bandwidth.

4. Gas-loaded, free-electron laser.

Although every spontaneous source has the possibility of becoming stimulated, the parameter values for the three previously discussed approaches are such that it would be difficult to achieve stimulated emission. As a final example, we will consider a process which is designed to be stimulated, and consists of adding a gas to the wiggler section of a free-electron laser.[13] For specified wiggler parameters and optical wavelength, the addition of a gas reduces the phase velocity of the wave and thereby permits a reduction in γ. The attendant advantages over the vacuum free-electron laser are:

(1) Higher gain per unit length.
(2) Lower cost and size for the electron accelerator.
(3) Wavelength tuning by varying the gas pressure.

If the interaction occurs near a resonant transition in the gas, it is possible to obtain some very interesting characteristics, as shown in Table III. In the visible spectrum, using the Li resonance, the power gain can be as high as 11 db per pass, and for the VUV transition in He a single pass gain of 50% is achievable with γ = 80 particles. This latter result should be contrasted with the GeV storage ring required for the vacuum FEL case.

Table III.

Parameters for a gas-loaded, FEL operating near an electronic resonance in a gas. P is the gas pressure in Torr, T is the gas temperature in K, L is the interaction length in cm., K^2 is the wiggler parameter, Net Gain is the single pass gain after absorption losses have been subtracted, ε is the beam emittance in mm-mrad, and $\Delta E/E$ is the percent energy acceptance for the electron beam.

Resonant GFEL Parameters

I = 15A γ = 80

Meduim	λ(Å)	P(Torr)	T(K)	L(cm)	K^2	NET Gain(%)	Beam Requirements ε(mm-mrad)	$\Delta E/E$(%)
Li	6775	4.6	1110	80	3	500 (11db)*	1.0	0.3
He	590	50	300	20	1	50	0.1	0.1

* Gain from exponential theory.

The primary disadvantage to the addition of a gas is the increased angular divergence of the electrons caused by multiple scatterings from the hydrogen molecules. This limits the interaction length, and this is the mechanism for determining the lengths listed in Table III. However, the gain per unit length is sufficiently large so that this is not a significant handicap, and the ability to use a short wiggler section has the advantages of reducing the requirements on input beam quality, allowing for easier alignment of the wiggler, and reducing the size and cost of the wiggler.

This work has been supported by: DOE #DEFG-03-84-ER13275, AFOSR #AFOSR-81-0209, and JSEP #DAAG-29-81-K-0057.

References:

1. V.L. Ginzburg and I.M. Frank, J. Phys. (USSR) 9, 353 (1945).
2. G.M. Garibyan, Sov. Phys. JETP 6, 1079 (1958).
3. M.L. Ter-Mikaelian, Nucl. Phys. 24, 43 (1961).
4. M.A. Piestrup, J.O. Kephart, H. Park, R.K. Klein, R.H. Pantell, P.J. Ebert, M.J. Moran, B.L. Berman, and B.A. Dahling, to be published in Phys. Rev. A., Sept. (1985).
5. R.H. Pantell, Stanford University proposal to DARPA, SSEL 12-83 (1983).
6. J.U. Andersen, E. Bonderup and R.H. Pantell, Ann. Rev. Nucl. Part. Sci. 33, 453 (1983).
7. R.H. Pantell, H. Park, R.L. Swent, J.O. Kephart, R.K. Klein, S. Datz and B.L. Berman, IEEE Trans. Nucl. Sci., NS-30, 3150-3154 (1983).
8. H. Park, R.H. Pantell, R.L. Swent, J.O. Kephart, B.L. Berman, S. Datz, R.W. Fearick, J. Appl. Phys., 55, 358-364 (1984).
9. R.K. Klein, R.L. Swent, R.H. Pantell, H. Park, J.O. Kephart, B.L. Berman, S. Datz, R.W. Fearick, Phys. Rev. 31B, 68-92 (1985).
10. R.O. Avakyan, I.I. Miroschnichenko, J.J. Murray and T. Viqut, Sov. Phys. JETP 55, 1052 (1982).
11. Y.N. Adishchev, A.N. Didenko, V.V. Kaplin, A.P. Potylitsin, and S.A. vorobiev, Phys. Lett., 83A, 337 (1981).
12. V.A. Bazylev, V.I. Glebov, E.I. Denisov, N.K. Zhevago, M.A. Kumakhov, A.S. Khlebnikov and V.G. Tsinoev, Sov. Phys. JETP 54(5), 854, Nov. (1981).
13. R.H. Pantell, J. Feinstein, A.S. Fisher, T.L. Deloney, M.B. Reid, and W.M. Grossman, presented at the 7th International Free Electron Laser Conference at Lake Tahoe, Sept. 8-13, 1985.

Temperature Dependence of Planar Channeling Radiation

H. Park, J.O. Kephart, R.K. Klein, and R.H. Pantell
Department of Electrical Engineering
Stanford University, Stanford, CA 94305

M.V. Hynes
Los Alamos National Laboratory
University of California
Los Alamos, NM 87545

B.L. Berman
Department of Physics
The George Washington University
Washington, D.C. 20052
and
Lawrence Livermore National Laboratory
University of California
Livermore, CA 94550

B.A. Dahling
Lawrence Livermore National Laboratory
University of California
Livermore, CA 94550

S. Datz
Oak Ridge National Laboratory
Oak Ridge, TN 37830

R.L. Swent
Imatron, Inc.
South San Francisco, CA 94080

M.J. Alguard
Measurex, Inc., Cupertino, CA 95015

In this paper we report measurements of 54-MeV electron planar-channeling radiation spectra as a function of temperature, down to liquid-nitrogen temperature, for a silicon crystal.

For electron channeling, the thermal vibration of the atoms, which causes transitions between bound eigenstates as well as dechanneling, is the primary contributor to the linewidth (Ref.1). At lower temperature the linewidth is reduced, since the thermal vibration of the atoms decreases with temperature. Another effect of cooling is to shift the spectral lines to higher frequencies. The potential well for a fixed atom is deeper than the corresponding well for a vibrating atom, and in the former case there is greater separation between the energy eigen- values. Figure 1 shows the silicon (110) planar potential at 80 K and 293 K.

The measurements reported here were done with 54-MeV electrons from the Lawrence Livermore National Laboratory Electron-Positron Linear Accelerator. Details of the experimental setup can be found in Ref. 1. In the present experiment, a 19-μm thick, <100> axis silicon crystal was mounted on a copper cold finger which was clamped to a small refrigerator (Ref. 2). The whole system was mounted in our goniometer, in which heat exchange with the surroundings was by radiation only and was minimal. The crystal temperature was monitored by two thermometers: one was built into the refrigerator and the other one was attached to the silicon crystal. Both yielded temperature readings within 1° of each other, showing that the thermal load was well within the capacity of the refrigerator.

Figure 2 shows the 54-MeV electron channeling-radiation spectra from the (100) and (110) planes at room temperature and at low temperature. The heavy dots are the low-temperature data [-190°C for the (100) plane and -180°C for the (110) plane], and the light dots are the room-temperature data. One can observe a

is substantially lower than the value of 543 K obtained earlier by Batterman and Chipman from their x-ray-diffraction data (Ref. 3). A value of 543K for Dabye Temperature gives the dashed lines in Figures 3 and 4, which lie well outside the experimental uncertainty.

A possible source of error in our determination of the Debye temperature may be inherent in the use of an average crystal potential. In calculating peak energies in planar channeling radiation, one starts with the planar-averaged potential. Assuming a Gaussian distribution of atoms, one can get the final form of the potential. From the potential one then can calculate the radiation peak energies (Refs. 7 and 8) easily and conveniently. This procedure gives excellent agreement between the measured and calculated transition energies for diamond (Ref. 1), Ge (Ref.9), and GaAs (Ref. 10). However, the rigorous approach is to solve the Schroedinger equation for the frozen lattice sites at different times and to average the peak energies subsequently. This method is quite complicated, but should be looked into to see whether it yields a different value.

Our measured linewidths are compared with our calculated values in Figs. 5 and 6. For both planes the agreement is reasonably good. In the calculation three line-broadening mechanisms were included: Bloch-wave broadening, Doppler broadening due to multiple scattering, and lifetime broadening. [Other line-broadening effects that we have considered are minor and do not affect our calculation in any significant way (Ref. 1).] The values for the linewidths from these three effects were added in quadrature to produce the values shown in Figs. 5 and 6. Generally, one can expect that the linewidth would broaden as the temperature increases, due to the increase of multiple scattering. The other two effects considered here do not vary as the temperature changes.

Figure 7 shows the experimental values of Ref. 5 compared

References:

1. R.K. Klein, J.O. Kephart, R.H. Pantell, H. Park, B.L. Berman, R.L. Swent, S. Datz, and R.W. Fearick, Phys. Rev. B 31, 68 (1985).

2. MMR Technology, Inc., Mountain View, CA.

3. D.S. Gemmell, Rev. Mod. Phys. 46, 129 (1974).

4. G. Dolling and R.A. Cowley, Proc. Roval Soc. 88, 463 (1966).

5. J.U. Andersen, E. Laegsgaard, and A.H. Sorensen, Nucl. Instrum. Methods B2, 63 (1984).

6. O.H. Nielsen and W. Weber, J. Phys. C: Solid State Phys. 13, 2449 (1980).

7. B.W. Batterman and D.R. Chipman, Phys. Rev. 127, 690 (1962).

8. J.U. Andersen, K.R. Eriksen, and E. Laegsgaard, Phys. Scripta 24, 588 (1981).

9. H. Park, R.L. Swent, J.O. Kephart, R.H. Pantell, B.L. Berman, S. Datz, and R.W. Fearick, Phys. Lett. 96A, 45 (1983).

10. H. Park, J.O. Kephart, R.K. Klein, R.H. Pantell, B.L. Berman, and S. Datz, submitted to Appl. Phys. Lett.

Table II. Channeling-radiation peak energies as a function of temperature for 54.4-MeV electrons channeled along the (110) planes of silicon.

Transitions	Measured							Calculate
	7°C	0°C	-40°C	-80°C	-89°C	-140°C	-180°C	
1 → 0	121.4 ±1.5	122.0 ±1.2	122.8 ±2.0	127.0 ±2.0	129.5 ±1.5	131.9 ±1.5	134.3 ±1.5	125.4 142.3
2 → 1	87.3 ±1.2	86.6 ±1.0	86.8 ±1.0	88.2 ±1.0	88.3 ±1.0	87.5 ±0.8	87.1 ±0.8	90.3 93.4
3 → 2	63.1 ±1.0	62.6 ±1.0	61.9 ±0.8	62.9 ±0.8	63.3 ±0.8	62.2 ±0.8	62.8 ±0.8	65.4 65.0
4 → 3	47.8 ±1.0	48.1 ±0.8	48.1 ±0.8	48.5 ±0.8	48.6 ±0.8	48.4 ±0.6	48.0 ±0.8	50.0 50.4
5 → 4	37.6 ±1.0	37.4 ±1.0	36.6 ±1.0	37.1 ±0.8	37.6 ±0.6	36.8 ±0.8	36.9 ±0.6	38.8 38.7

* Two values are for two extreme temperatures. The first one is for 7°C and the second one is for -180°C. 495 K of Debye temperature is used in calculation.

Fig. 5 Measured and calculated channeling-radiation linewidths as a function of temperature, for 54.4-MeV electrons channeled along the (100) planes of silicon. In the calculation, a Debye temperature of 495 K was used. Squares are for 3→2 transitions and triangles are for 2→1 transitions.

Fig. 6 Measured and calculated channeling-radiation linewidths as a function of temperature, for 54.4-MeV electrons channeled along the (110) planes in silicon. In the calculation a Debye temperature of 495 K was used.

Fig. 7 Measured and calculated 3P→1S and 2P→1S transitions of 3.5 MeV electron axial channeling radiation for <111> axis of silicon as a function of temperature (experimental data from Ref. 5). The solid lines were calculated using two different Debye temperatures, for comparison.

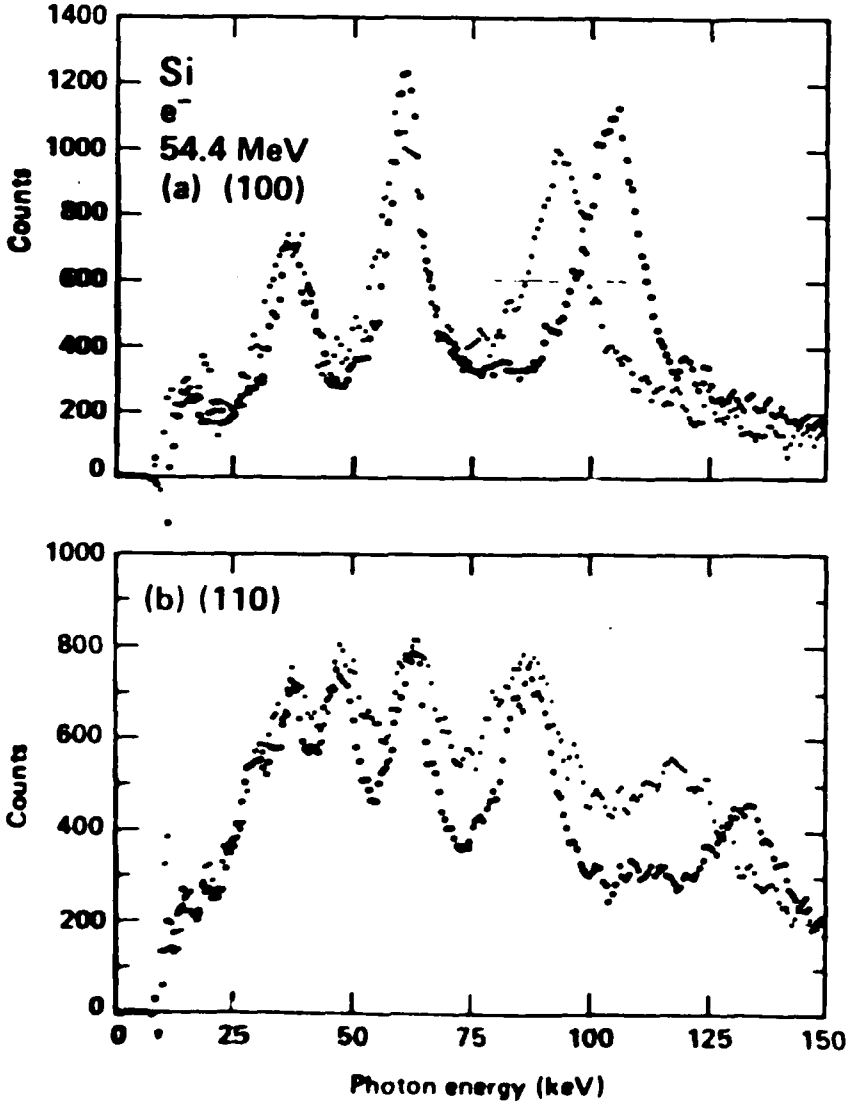
Si
e⁻
54.4 MeV
(a) (100)
(b) (110)
Counts
Counts
Photon energy (keV)
0
200
400
600
800
1000
1200
1400
25
50
75
100
125
150

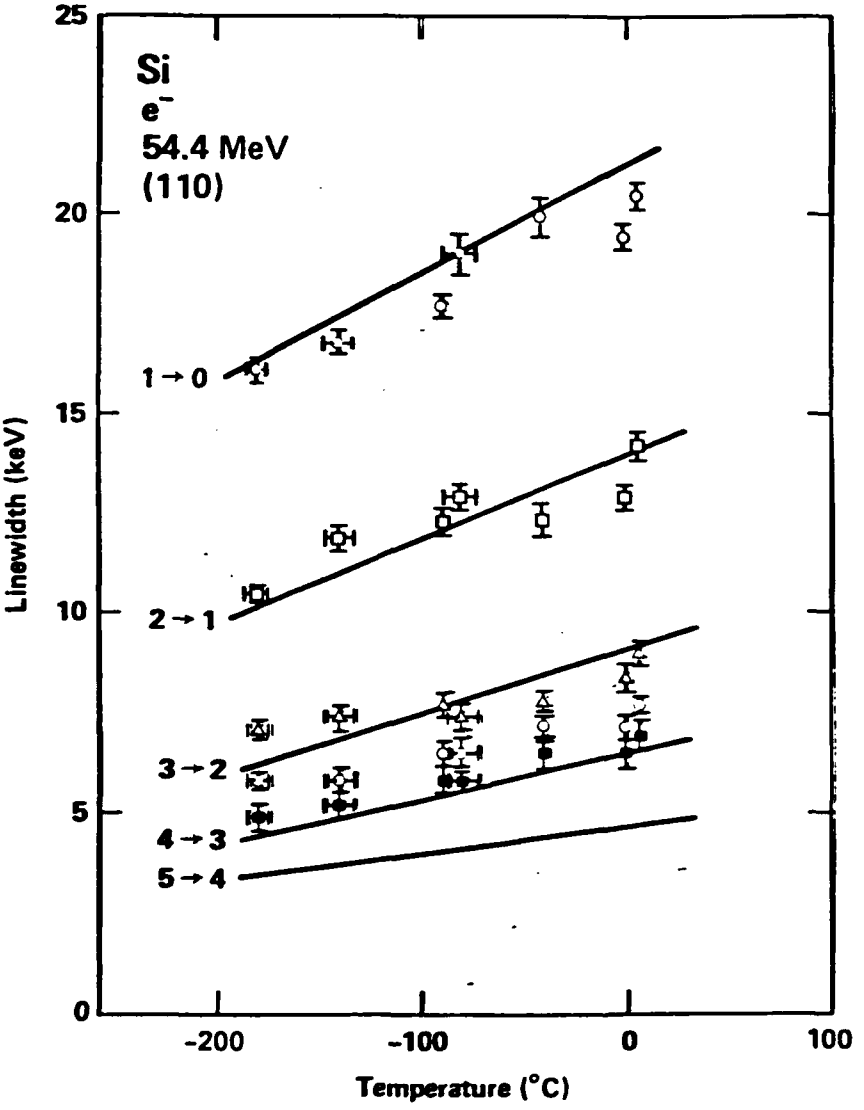
Si
e⁻
54.4 MeV
(110)
1 → 0
2 → 1
3 → 2
4 → 3
5 → 4
Linewidth (keV)
Temperature (°C)
25
20
15
10
5
0
-200
-100
0
100

END

4-1-87

DTIC